Estimation of Rail Irregularities

by

Junji Kawasaki

M.Eng. Engineering Synthesis
The University of Tokyo, 1993

Submitted to the Department of Mechanical Engineering
in Partial Fulfillment of the Requirements for the Degree of
Master of Science in Mechanical Engineering

at the

Massachusetts Institute of Technology

JUNE 2001

Signature of Author .....
Department of Mechanical Engineering
May 11, 2001

Certified by .....
Kamal Youcef-Toumi
Professor of Mechanical Engineering
Thesis Supervisor

Accepted by .....
Ain A. Sonin
Chairman, Department Committee on Graduate Students

Estimation of Rail Irregularities

Junji Kawasaki

Submitted to the Department of Mechanical Engineering on May 11, 2001
in Partial Fulfillment of the Requirements for the
Degree of Master of Science in Mechanical Engineering

Abstract

Inspection cars that have been used to measure rail irregularities are costly and need operators. This thesis proposes a method to estimate rail irregularities by measuring accelerations of a passenger car instead of direct measurement by using a conventional inspection car.

Using a System Identification technique and data obtained by simulations based on a three-dimensional rail vehicle model with actual rail irregularities, the proposed method identifies an inverse system where inputs are accelerations of a vehicle and outputs are rail irregularities. The resulting model is assessed through comparing the estimated irregularity with the actual irregularity. Validation results show that the estimate agree well with the actual irregularity for the Vertical Irregularity. Though the estimation error for the Lateral Irregularity is larger than that for the Vertical Irregularity, the error is acceptable form a practical point of view. The quality of the estimation is evaluated quantitatively by using the Mean Square Error. In addition, resolution of the estimation is presented in order to demonstrate the accuracy of the estimation.

Model uncertainties are assessed for a practical implementation. The effects due to two major uncertainties, mass variations and speed variations, are evaluated by using the Singular Value Decomposition in order to present the limitations of the estimation using a nominal model. In addition, this thesis proposes a compensation method for mass variations and speed variations.

Thesis Supervisor: Kamal Youcef-Toumi
Title: Professor of Mechanical Engineering

Acknowledgements

First of all, I would like to thank Prof. Kamal Youcef-Toumi, my thesis adviser for giving me the opportunity to work on this project. I am really grateful for his advice and patience throughout this thesis project.

I also would like to thank East Japan Railway Co., which gives me the opportunity to study at MIT and supports financially. Thanks to Prof. Joseph Sussman, Professor of Civil and Environment Engineering, JR-East Professor, who arranged the environment for me to study comfortably.

Thanks to Mr. Koizumi of Sumitomo Metal Co., who provided me with useful data for simulations and precious comments on my work.

My friends in Mechatronics Laboratory and Advanced Study Program deserve my special gratitude for all those interesting discussions for my research.

Thanks to my family, Yuki and Shunsuke, for everything. Without your support, patience and encouragement, none of this work would have been possible.

TABLE OF CONTENTS

LIST OF FIGURES

LIST OF TABLES

1 Introduction

1.1 Problem Statement

Railroad companies spent a large amount of money on maintenance of facilities such as railway tracks, rolling stocks and station buildings. Therefore, reduction of maintenance work is a matter of great interest to them. In particular, maintenance of railway tracks has been among the most laborious work since the railroad system was invented. On the other hand, the maintenance of railway tracks has been extremely important for both safety and service for passengers. Rail irregularities cause deterioration of riding comfort. Derailments that endanger passengers have occurred because of rail irregularities.

Rail maintenance work consists of measuring irregularities and adjusting the alignment of rails. Both parts had been done manually by maintenance workers until inspection cars and multiple tampering machines were developed. Inspection cars are equipped with special mechanisms and sensors for measuring. However, railway maintenance by using inspection cars is costly because inspection cars themselves are expensive and still need operators.

Some approaches have been researched to reduce the cost of inspection cars and to realize a higher accuracy of measurement [1,2,3,4,5,6,7 and 8]. Recently the idea that regular passenger cars could be used for measurement of rail irregularities has started to be researched. Because passenger cars that measure rail irregularities would not need any special inspection car and operators, they would produce a more frequent and labor-saving rail inspection.

Takeshita [9] proposed a method using passenger cars instead of inspection cars. In the method, an accelerometer is mounted on an axle box for detecting vertical irregularities. The estimate is calculated by the double integration of the accelerations. However, the double integration of the accelerations is unstable for low-frequency irregularities, because the gain of the double integration becomes large at low frequencies. The study proposes the design of a high-pass filter to solve this problem. Optical sensors and gyros are mounted on a bogie to measure other types of irregularities. Optical sensors measure the position of a rail by using reflection of a light from the rail. Gyros estimate the level irregularity by measuring the angle of the bogie. The results of the estimation and comparisons with the actual irregularity have not been presented by this method.

Bryan [10] proposed a method using onboard sensors such as tilt sensors and accelerometers that detect rail abnormalities such as broken rails, weak rail ties and cracked rails. Measured accelerations and angular movement information of the vehicle are simply compared with historical status data instead of estimating the rail irregularity. The results of the estimation and comparisons with the actual irregularity have not been presented by this method.

The above methods have some practical problems. First, using sensors on the axle box and on the bogie instead of a car body deteriorates the accuracy of the measurement, because it is not a good environment to place sensors. Next, using many sensors is costly. So as to take more advantage of the merit of using passenger cars instead of costly inspection cars, less costly methods should be researched. In addition, comparing the estimate with the actual irregularity is needed to assess methods of estimating the rail irregularity.

This thesis uses only accelerometers, which is costless, because one of the objectives is to propose a costless method instead of using conventional inspection cars and operators. The accelerometers are placed on the floor of a vehicle instead of an axle box and a bogie. In addition, this study presents the results of the estimation and comparison with the actual irregularity. To estimate the rail irregularity with the acceptable error by a costless method is one of technical challenges.

The idea of using a passenger car's vibrations for estimating rail irregularities is in a sense contradictory to the concept of suspensions that absorb vibrations. If the ideal suspension absorbed vibrations completely, the idea of estimating rail irregularities from car vibrations would never be realized. However, such an ideal suspension has never been developed and the main idea of this thesis deserves study. Therefore, to understand how we can retrieve information of rail irregularities from vehicle vibrations that are alleviated by suspensions is another technical challenge.

1.2 Objectives of the Thesis

The main objective of this thesis is to propose a method for estimation of railway irregularities by measuring the accelerations of a passenger car. While an actual system has inputs of rail irregularities and outputs of a vehicle's vibrations, the system that this project considers has an inverted relationship of inputs and outputs. An important technical challenge of this thesis is dealing with the inverted relationship of inputs and outputs.

Since there has been no work that presents the results of comparisons between the estimate and the actual rail irregularity by using a passenger car, we cannot quantitatively compare the method proposed by this thesis with others. However, it will be important to quantitatively evaluate the estimation results in order to practically implement this thesis's method. Therefore, to present a method for evaluation of the estimation results is one of this thesis's objectives.

In addition, considerations for system uncertainties are needed. Generally, it is very rare for a system to possess no uncertainty. A system usually has some properties that cannot be mathematically dealt with and variations of parameters. Therefore, this thesis must consider effects produced by some uncertainties and propose a method to compensate for the effects.

1.3 Thesis Outline

This thesis proposes a method for estimation of rail irregularities by measuring accelerations of a passenger vehicle. In Chapter 2, the definitions of the rail irregularities are presented. In addition, Chapter 2 outlines selection of a software package of a rail vehicle's dynamics simulation and modeling of components of a rail vehicle. Chapter 3 details a method for the estimation of rail irregularities and presents evaluations for the accuracy of the estimation. Chapter 4 assesses the effects due to model uncertainties such as mass variations and speed variations. Chapter 5 presents conclusions and recommendation for future work.

2 Rail Irregularities and Vehicle Dynamics

2.1 Introduction

Basics for estimating rail irregularities are presented in this chapter. Definitions of rail irregularities and an outline of simulation that generates data for their estimation are presented. In addition, modeling of components of a vehicle is presented as well.

2.2 Rail Irregularity

2.2.1 Types of the Rail Irregularity

Rail tracks support weights of trains and help trains smoothly run. However, operations of trains cause gradual rail irregularities. The rail irregularity is an important item for maintenance work, because they can affect the riding quality and the safety of rail vehicles.

The absolute positions of two rails at any points can be defined by using four variables (I_{ll}, I_{vl}, I_{lr}, and I_{vr}), as shown in Figure 2.1. Because it is laborious and costly for railroad companies to measure the values of the four variables along lines in the absolute coordinate ($Y-Z$), they generally define four types of the rail irregularities [11]:

1) Irregularity of Line (I_a)

This is the irregularity in the lateral direction. The distance between a 10-meter string and a side surface of a rail, which is referred to as the Versine, represents the Irregularity of Line at a certain point in Figure 2.2 (a).

2) Vertical Longitudinal Irregularity (I_b)

This is the irregularity in the vertical direction. Similarly to the Irregularity of Line, the Versine represents the Vertical Longitudinal Irregularity, as shown in Figure 2.2 (b).

3) Level Irregularity (I_e)

This is a difference in the vertical direction between the right rail and the left rail at a certain point, as shown in Figure 2.2 (c).

4) Gauge Irregularity (I_g)

Figure 2.2 (d) shows the Gauge Irregularity. This is a deviation from the standard gauge, which is 1435 [mm].

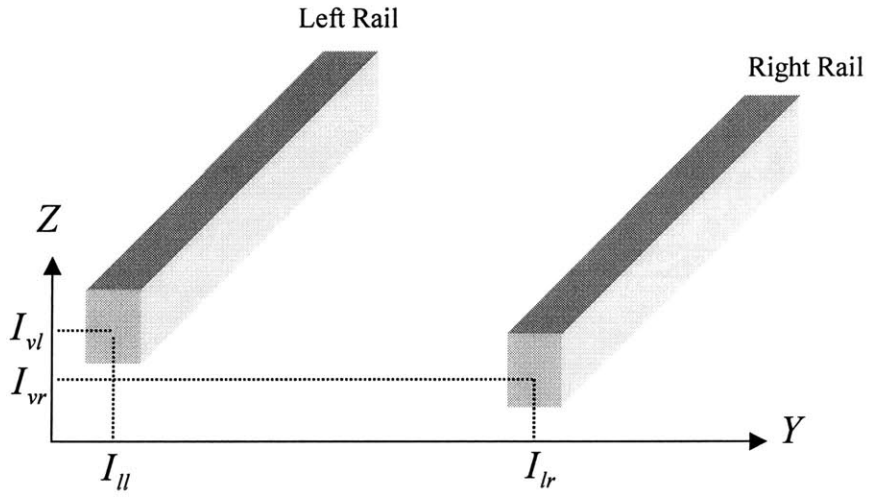

Figure 2.1 Absolute Positions of Rails

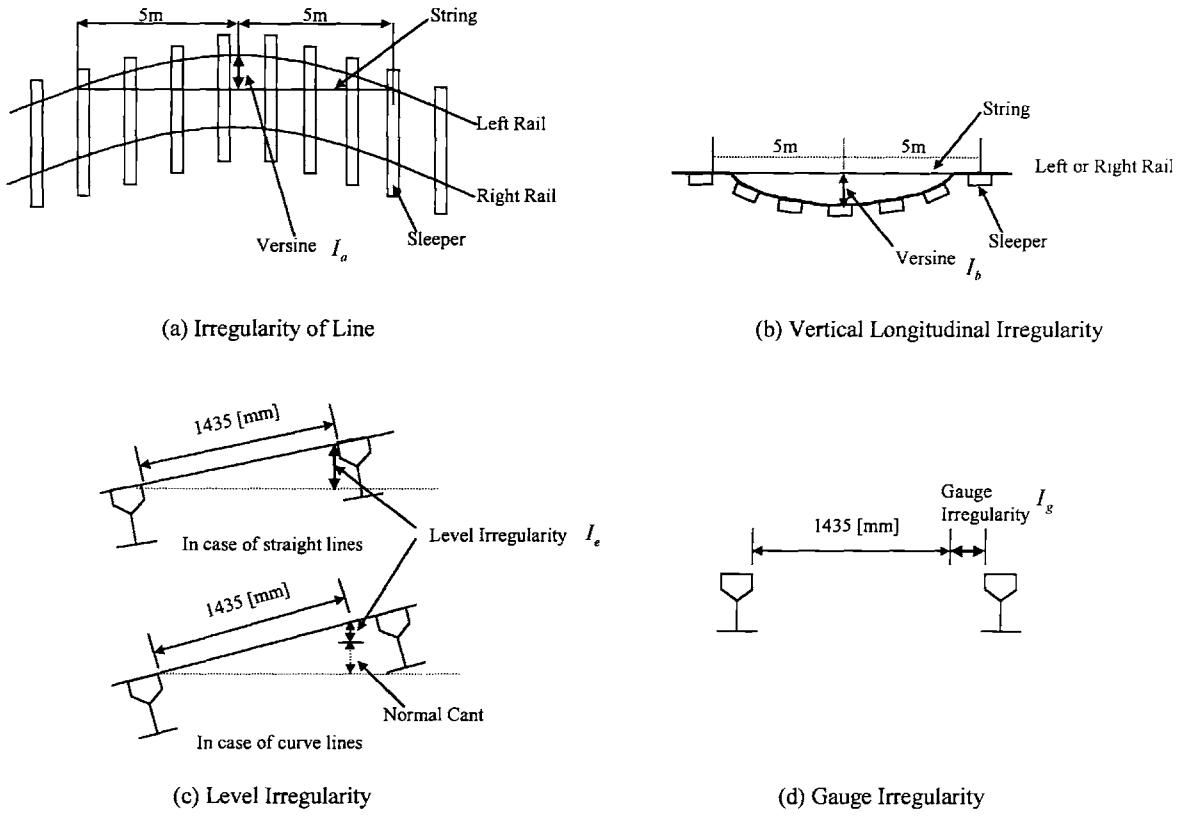

(a) Irregularity of Line

(b) Vertical Longitudinal Irregularity

(c) Level Irregularity

(d) Gauge Irregularity

Figure 2.2 Four Definitions of Rail Irregularity

The Irregularity of Line and the Vertical Longitudinal Irregularity are defined by using the Versine. Because the 10-meter Versine is a relative position based on two distant (5 meters) positions, it is not a position in the absolute coordinate. For example, if we have a sinusoidal irregularity whose wave length is 5 [m] on a rail, the irregularity cannot be detected by using the 10-meter Versine. On the contrary, when we have a sinusoidal irregularity whose wave length is 10 [m], the corresponding Versine is twice as much as the actual irregularity. Therefore, the gain of the Versine method depends on the irregularity's wave length.

A conventional inspection car uses three bogies. One of two wheelsets of the middle bogie is used to measure the Versine, while one of two wheelsets of the leading bogie and one of two wheelsets of the trailing bogie play a role as the both ends of a string. Since the Versine is not the actual irregularity, the digital filter is necessary in order to estimate the actual irregularity of a rail [12].

In this thesis, combined absolute positions in Figure 2.1 and conventional types of the irregularity, the following new definitions of the irregularity in Figure 2.3 will be used.

1) Left Lateral Irregularity (the lateral position of the left rail): I_{ll}
2) Left Vertical Irregularity (the vertical position of the left rail): I_{vl}
3) Level Irregularity: I_e
4) Gauge Irregularity: I_g

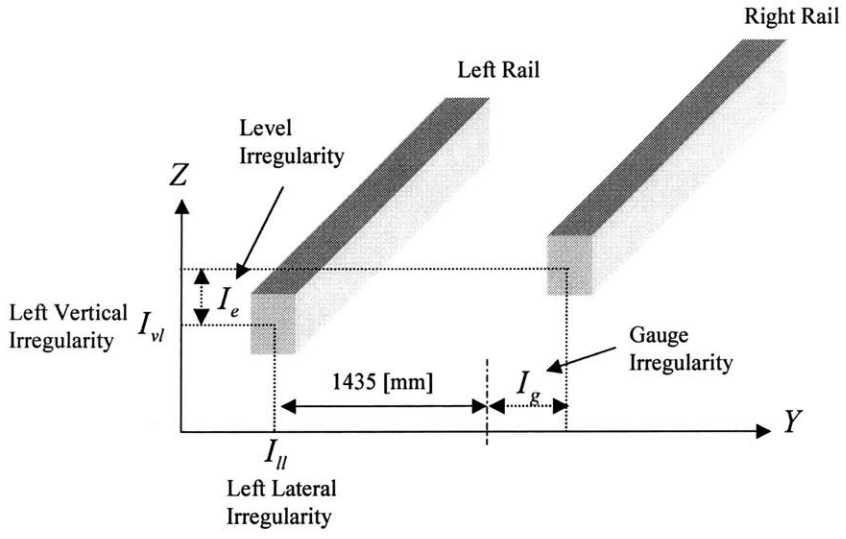

Figure 2.3 Definitions of Rail Irregularities

Table 2.1 shows the standard range of the rail irregularity for rail maintenance work [11]. If the rail irregularity is outside the standard range, alignment must be done. Table 2.1 shows the standard range for the rail irregularity, which is used for practical maintenance work. We will use the same standard for the irregularities defined in Figure 2.3. For example, the standard range of the irregularity of the conventional line is $1067 \pm 7[mm]$.

Table 2.1 Standard of Rail Irregularities

	Unit	The conventional line (1067[mm])	The Shinkansen Line (1435[mm])
Irregularity of Line	mm	7	4
Vertical Longitudinal Irregularity	mm	7	7
Level Irregularity	mm	7	3
Gauge Irregularity	mm	+3 -2	+3 -2

2.3 Simulation by Using a Vehicle Dynamics Software Package

2.3.1 Simulation Software Package

Because the main objective of this thesis is to estimate rail irregularities by using a vehicle's accelerations, data of accelerations that are caused by certain rail irregularities are needed. The idea of this thesis must be evaluated before utilization in field experiments. Therefore, simulation software package is adopted instead of experiments.

The following specifications are the requisites for the software package:

1) Rail Irregularities as system inputs

2) Three dimensional analysis

3) Arbitrary positioning of sensors to measure the positions, speeds and accelerations of a car body.

According the benchmark test for rail vehicle simulation [13], there are five major software packages. There are generally good agreements between them in the benchmark test. However, because the Gensys software package can deal with the elasticity of a wheel and a rail in the contact area, Gensys is selected to use.

2.3.2 Modeling of a Rail Vehicle

Since a rail vehicle is a complicated system, modeling of components is an important process [14]. Linearization of components is effective in some analyses. However, since we cannot expect how much effect linearization has for the estimation of rail irregularities, a lot of non-linear factors shall be included in the model. While Appendix A. details the properties of vehicle components, explanations on components and modeling in Gensys is outlined:

1) Rail Track

Rails are modeled as rigid bodies. Rails and ground points are coupled by stiffness (k_{gl}) and damping (c_{gl}) in the lateral direction, and stiffness (k_{gv}) and damping (c_{gv}) the vertical direction. Figure 2.4 shows these components.

2) Creep Force

Forces between wheels and rails are important factor in rail vehicle' dynamics. Unlike automobile's case, the surface between a wheel and a rail is not a plane but a curved surface. The force is referred to as the Creep Force.

In simulations, the Linear Creep Force Theory is used. The Creep Forces (T_1 and T_2) are proportion to the Creepage (ν_1 and ν_2), which is the slip speed of a contacting surface.

$$T_1 = \kappa_1 \nu_1$$

$$T_2 = \kappa_2 \nu_2$$

where κ_1 and κ_2 are the Creepage coefficients.

The Creepage is computed form the positions of the surface and the angle of the axle. The Spline Function interpolates the curves of a wheel tread and a rail surface to obtain the position of contacting surfaces and the angles of the contact in Gensys.

3) Wheelset

A wheelset is modeled as a rigid body that has a mass (M_w) and mass moments of inertia (J_{wr}, J_{wp}, and J_{wy}).

4) Bogie Frame

A bogie frame is modeled as rigid body that has a mass (M_b) and mass moments of inertia (J_{br}, J_{bp}, and J_{by}).

5) Primary Suspensions

Suspensions between a bogie frame and an axle are called Primary Suspensions. Primary Suspensions consist mainly of two Axle Springs. An Axle Spring has stiffness (k_{pv}, k_{pl}, and k_{px}) in the three directions and non-linear damping (c_{pv1}, c_{pv2}, and c_{pv3}) in the vertical direction. Damping in the lateral and the longitudinal directions are neglected.

6) Secondary Suspensions

Suspensions between a car body and a bogie frame are called Secondary Suspensions. Components of Secondary Suspensions are summarized. Unless otherwise specified, the property of stiffness or damping is linear.

- Air springs are modeled as three-directional stiffness (k_{av1} , k_{av2} , and k_{av3}) and damping (k_{al}) in the lateral direction.
- A traction rod, which transfers forces from a bogie to a car body, has stiffness (k_{tx} and k_{tl}) in the lateral and the longitudinal directions.
- A lateral damper is used to complement lateral damping, because air springs' lateral damping is not sufficient. It is modeled as a non-linear damping (c_{l1} and c_{l2}).
- Two yaw dampers, which prevent a hunting phenomenon and helps smooth movements in curves, consist of non-linear damping (c_{y1} and c_{y2}) in the yawing direction.
- A lateral bump stop, which prevents excessive movement of a bogie in the lateral direction, is modeled as nonlinear factor. When it works, it is modeled as a stiffness (k_{bl}).

7) A Car Body

A car body is modeled as a rigid body, which has a mass (M_c).

8) Passengers

A passenger is considered a mass of 80 [kg]. Mass of passengers is added to the weight of a car body, when mass variations of a vehicle are assessed in Chapter 4. The movement of passengers on the floor is ignored in this thesis.

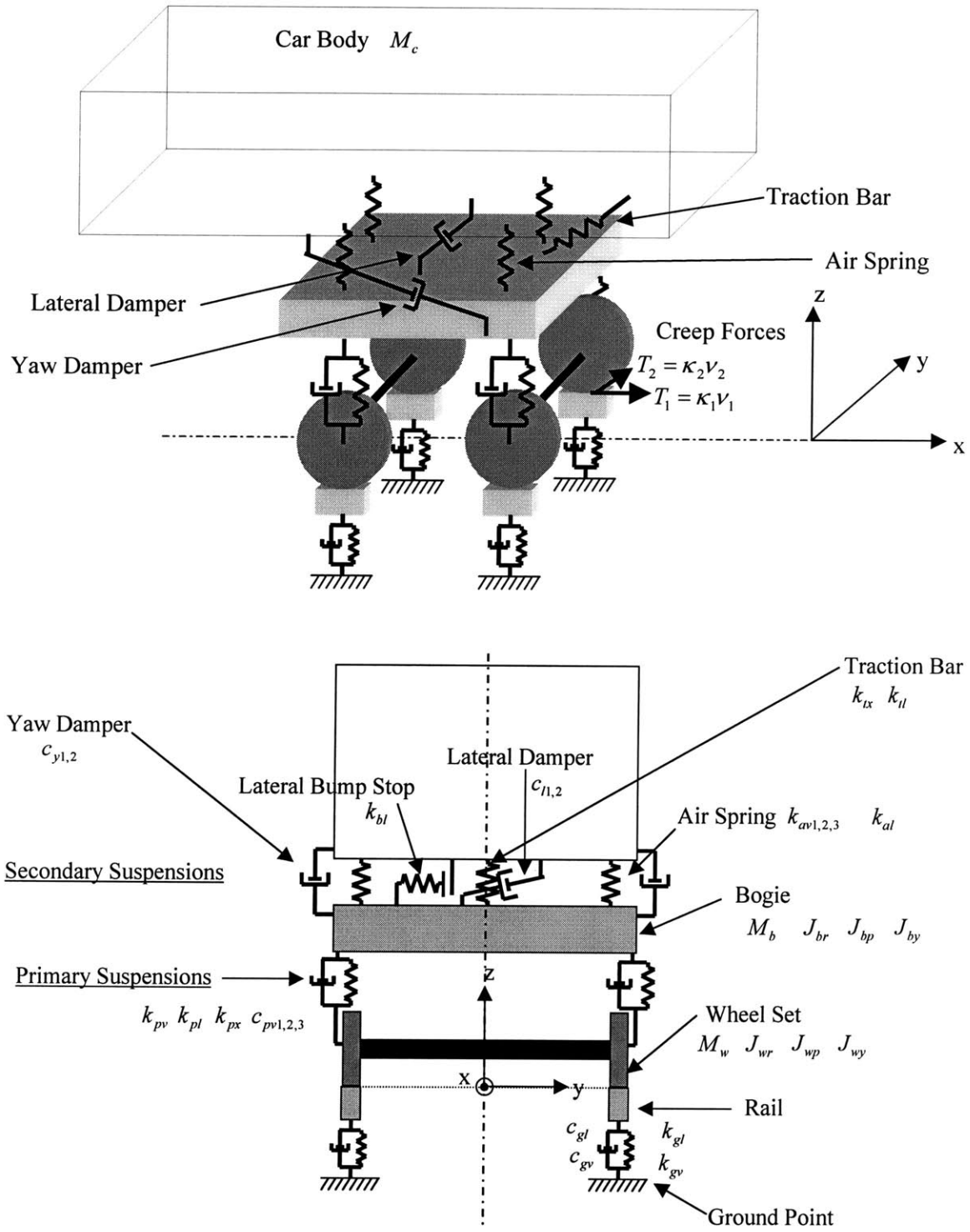

Figure 2.4 Modeling of a Rail Vehicle

2.4 Summary

This chapter outlines basics for proposing a method of estimating rail irregularities that is presented in the next chapter. Section 2.2 details definitions of rail irregularities. Since conventional definitions that have been used for maintenance work does not represent absolute positions, new definitions are presented. Section 2.3 outlines simulation by using a software package for rail vehicle's dynamics. Modeling of important components of a vehicle is summarized.

3 Estimation of Rail Irregularities

3.1 Introduction

This chapter proposes a method for estimation of rail irregularities. Section 3.2 details the method using a System Identification technique. Section 3.3 presents the results of the model construction. Section 3.4 presents validation of the resulting models in two methods. One method evaluates errors of estimates quantitatively. The other proposes a warning system for practical rail maintenance work.

3.2 System Identification of an Inverse Model

3.2.1 An Inverse Model

In an actual vehicle system, rail irregularities can be considered as inputs and vehicle vibrations can be considered as outputs. Because the objective of this thesis is to estimate rail irregularities, inputs and outputs need to be inverted, as shown in Figure 3.1. Thus, the main objective of this section is to identify this inverse model.

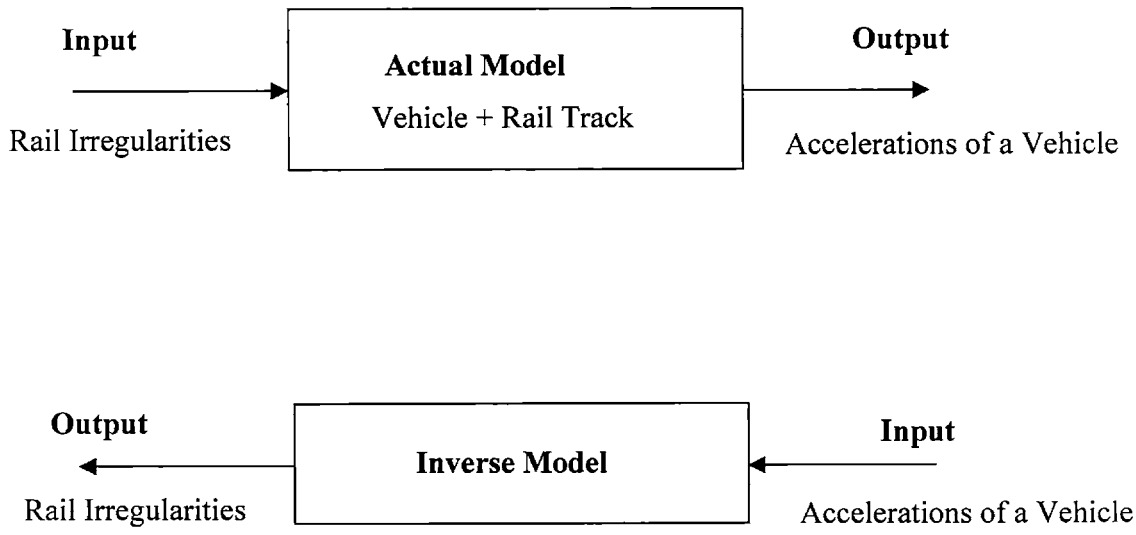

Figure 3.1 The Actual Model and an Inverse Rail Vehicle System

Before proceeding to a method to identify the inverse model, it is important to consider causality of a system. A system is said to be *causal* if the output at any time depends only on values of the inputs at the present time and in the past [22].

Figure 3.2 shows lateral irregularities and lateral accelerations of a car body for a SISO system, where there is no other irregularity. For example, some peaks of the lateral acceleration from 33 [sec] to 35 [sec] follows some peaks of the lateral irregularity from 30 [sec] to 33 [sec]. The lateral accelerations are attenuated after 35 [sec], because the lateral irregularities are getting small from 33 [sec] to 42.5 [sec]. The arrow in the figure shows causality between input and output. Thus, car body accelerations of an actual vehicle model depend on the rail irregularities at the present time and in the past.

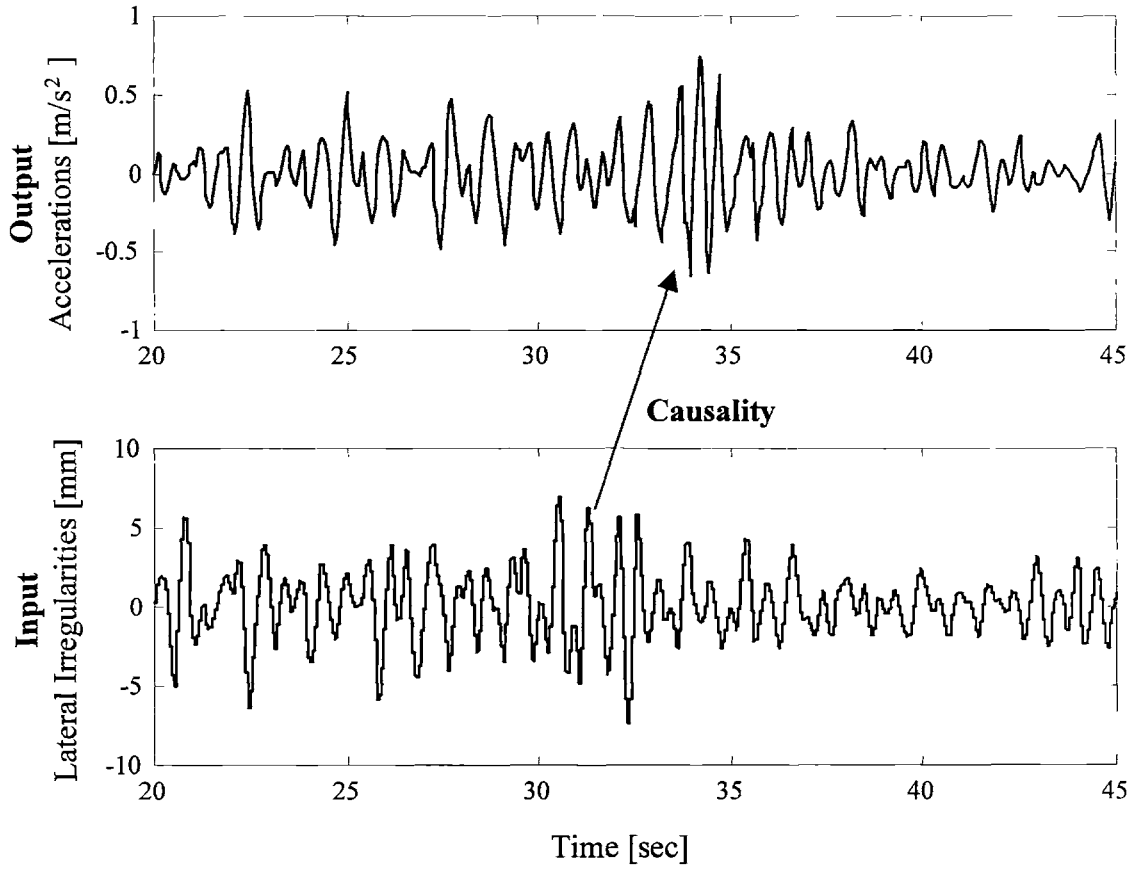

Figure 3.2 Causality between Rail Irregularities and Car Body Accelerations

Although we need to exchange inputs and outputs to realize an inverse model, the operation of simply exchanging inputs and outputs loses causality in the inverse system. Therefore, the order of data of inputs and outputs in the inverse system is reversed in the time axis. The inverse system is ready to catch causality, if there is causality between input and output. Figure 3.3 shows an example of reversing data in the time axis. Figure 3.3 (a) shows the lateral accelerations, $\mathbf{a}(t)$ where $0 \le t \le 100$ [sec], response to the three rail irregularities (lateral, vertical and level). Figure 3.3 (b) shows the lateral accelerations $\overline{\mathbf{a}}(t)$ reversed in time, that is $\overline{\mathbf{a}}(t) = \mathbf{a}(t_f - t)$, where t_f is the final time.

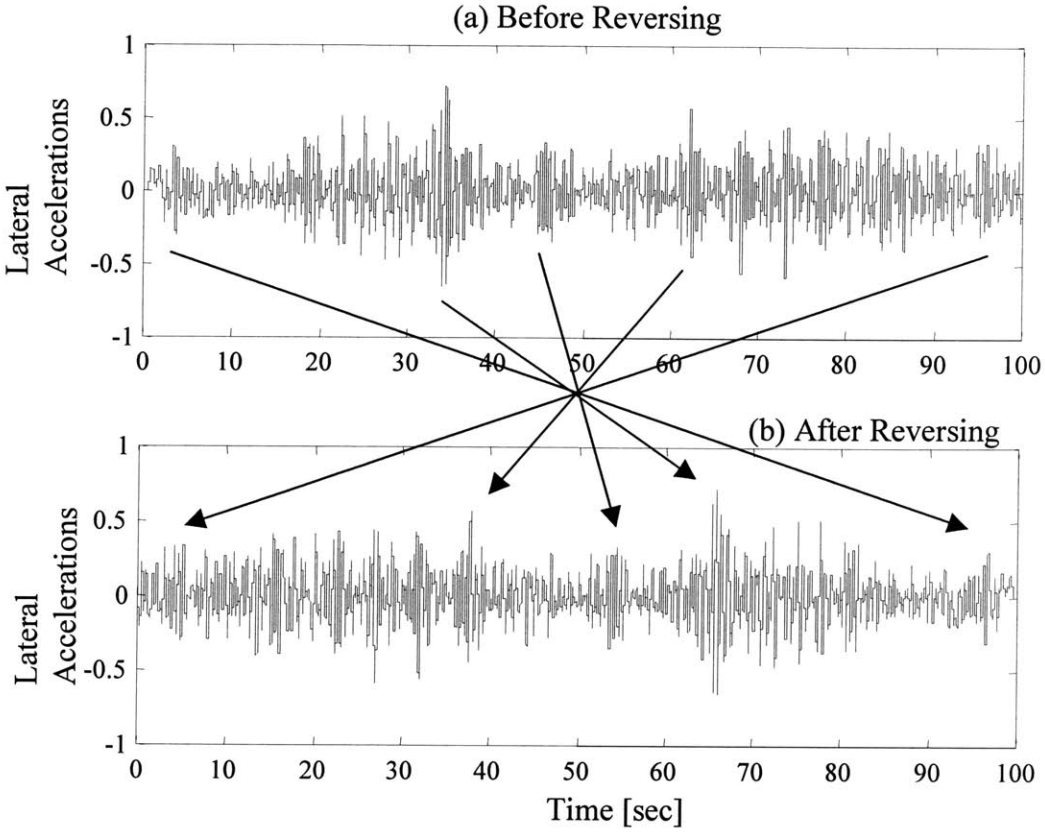

Figure 3.3 Reversing the Order of Data in the Time Axis for Causality

We have a system whose inputs are accelerations of a car body, outputs are rail irregularities, and time axis has the reverse order of the actual order. Therefore, the order shall be reversed again after estimation by a method that this thesis proposes.

3.2.2 The ARX Model

As mentioned in Chapter 2, dynamics of a rail vehicle contain both linear and nonlinear properties. However, the dynamics in the vertical direction are almost linear [14]. Although the effects of nonlinear properties in the lateral direction cannot be

ignored, in this thesis we shall consider linear models for simplicity. The nonlinear property will be considered as one of the model's uncertainties.

A generalized model structure of a SISO linear discrete system is expressed [15] as,

$$A(q)y(t) = \frac{B(q)}{F(q)}u(t) + \frac{C(q)}{D(q)}e(t) \tag{3.1}$$

where

q^{-1} is the delay operator,

$u(t)$ is the system's input,

$y(t)$ is the system's output,

$e(t)$ is the system's disturbance, and

A, B, C, D, and F are polynomials.

The simplest input-output relationship is obtained by describing it as a linear difference equation:

$$y(t) + a_1 y(t-1) + ... + a_n y(t-n) = b_1 u(t) + b_2 u(t-1) + ... + b_m u(t-m+1) + e(t) \tag{3.2}$$

Equation (3.2) can be expressed as,

$$A(q)y(t) = B(q)u(t-k) + e(t) \tag{3.3}$$

where

$A(q) = 1 + a_1 q^{-1} + ... + a_n q^{-n}$,

$B(q) = b_1 + b_2 q^{-1} + ... + b_m q^{-m+1}$, and

k is the number of delays from input to output. This model is called the Auto-Regression model with eXtra inputs (ARX).

The next step is to estimate parameters in Equation (3.3) by using data obtained in simulations or experiments. If we introduce the parameter vector θ :

$$\theta = [a_1 \cdots a_n \quad b_1 \cdots b_m]^T \tag{3.4}$$

and the regressor vector $\varphi(t)$:

$$\varphi(t) = [-y(t-1) \cdots -y(t-n) \quad n(t-1) \cdots u(t-m)]^T \tag{3.5}$$

then Equation (3.3) can be rewritten as

$$y(t) = \varphi^T(t)\theta . \tag{3.6}$$

In order to estimate the parameters in Equation (3.4), the Prediction Error Method (PEM) is used. A quadratic performance measure V is defined as:

$$V_N(\theta, Z^N) = \frac{1}{N}\sum_{i=1}^{N}\frac{1}{2}\varepsilon^2(i,\theta) \tag{3.7}$$

where

N is the number of data,

$Z^N = \{u(1), y(1), \ldots, u(N), y(N)\}$, which is a data set from simulations, and

$\varepsilon(i,\theta) = y(i) - \hat{y}(i \mid \theta)$,where $\hat{y}(i \mid \theta)$ is the estimate of $y(i)$ using a parameter vector θ, denotes the prediction errors. The parameter vector estimates

$$\hat{\theta}_N = \arg\min_{\theta} V_N(\theta, Z^N) .$$

Since V_N of Equation (3.7) is quadratic in θ, we can find the minimum value easily by setting the derivative to zero:

$$0 = \frac{d}{d\theta}V_N(\theta, Z^N) = \frac{2}{N}\sum_{i=1}^{N}\varphi(i)(y(i) - \varphi^T(i)\hat{\theta}_N)$$

which gives

$$\hat{\theta}_N = \left[\sum_{i=1}^{N}\varphi(i)\varphi^T(i)\right]^{-1}\sum_{i=1}^{N}\varphi(i)y(i) . \tag{3.8}$$

Consequently, $\hat{\theta}_N$ is analytical function provided that $\sum_{i=1}^{N}\varphi(i)\varphi^T(i)$ is invertible. Since

$$\frac{d^2}{d^2\theta}V_N(\theta,Z^N)=\frac{1}{N}\sum_{i=1}^{N}\varphi(i)\varphi^T(i),$$

this is ensured if $\frac{d^2}{d^2\theta}V_N(\theta,Z^N)$ is positive definite. In general, in other cases than the ARX, the predictor $\hat{y}(t)$ is not linear in θ and we cannot derive analytical expressions for the parameter estimate $\hat{\theta}_N$. Instead, we must use numerical search algorithms [16].

To ensure $\sum_{i=1}^{N}\varphi(i)\varphi^T(i)$ in Equation (3.8) is invertible, it is important to prepare informative experiments. Inputs must excite sufficiently the system. Therefore, it is important to prepare inputs whose magnitudes and frequencies cover whole the range where the system is practically used.

3.2.3 Vehicle Dynamics Simulation for System Identification

To estimate the parameters in a model using the ARX model with the PEM technique, data were collected in simulations. Table 3.1 details the conditions of the simulations. Appendix A. details the properties of a vehicle used in the simulations.

Table 3.1 Conditions of Vehicle Running Simulations

Item	Value
Vehicle Type	E2
Bogie Type	TR7004A
Gauge	1435[mm]
Track Geometry	Tangent
Rail Irregularities	Data from the Chuo Line, Japan
Speed	72 [km/h] (20 [m/s])
Total Distance	10,000 [m]
Distance for Model Construction	8,000 [m]
Distance for Model Validation	2,000 [m]
Data Sampling Rate	20 [Hz]

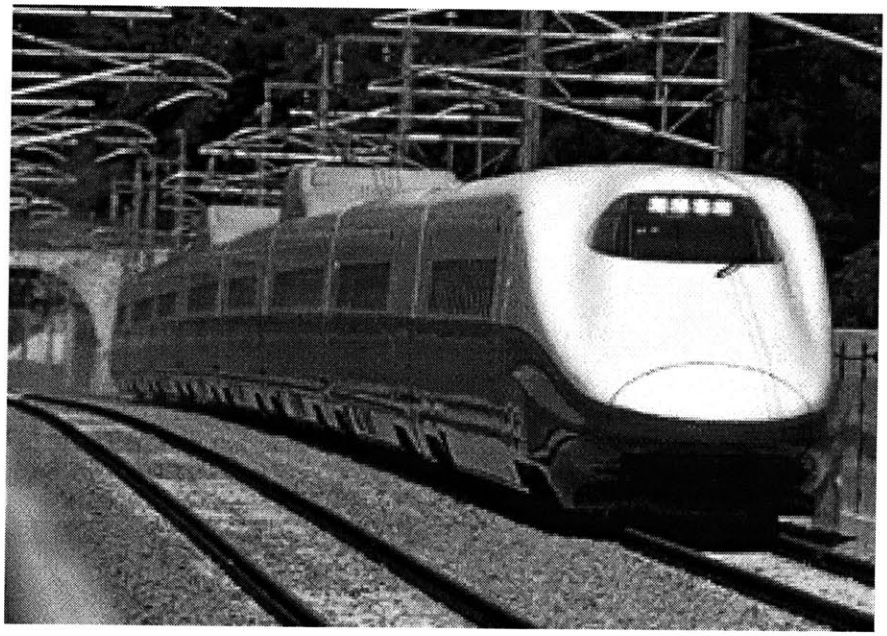

Figure 3.4 E2 Type Shinkansen Train

We consider the location of the accelerometers. At the first attempt, two accelerometers were placed in the middle of the vehicle's floor, as shown in Figure 3.5 (a). One was for the lateral accelerations (A_{lm}) and the other was for the vertical

accelerations (A_{vm}). Since there was no accelerometer to detect the accelerations associated with Level Irregularities, we could not detect Level Irregularities.

Next, three accelerometers were placed in the middle of the vehicle's floor, as shown in Figure 3.4 (b). Two accelerometers for the left lateral accelerations (A_{ll}) and the left vertical accelerations (A_{vl}) were placed on the left side of the middle of the vehicle's floor. The other for the right vertical accelerations (A_{vr}) was on the right side of the middle of the vehicle's floor. The difference between the vertical accelerations on the left side and on the right side ($A_{vr} - A_{vl}$) can be associated with Level Irregularities. Forces generated by rail irregularities were transferred to the vehicle through the bogies. Since there is a distance from the leading bogie to the middle of the vehicle, accelerations in the middle of the vehicle is attenuated and has a time delay. Therefore, we place the three accelerometers on the vehicle's floor over the leading bogie, which is the first point excited by the rail irregularities. Figure 3.4 (c) shows the final locations of three accelerometers.

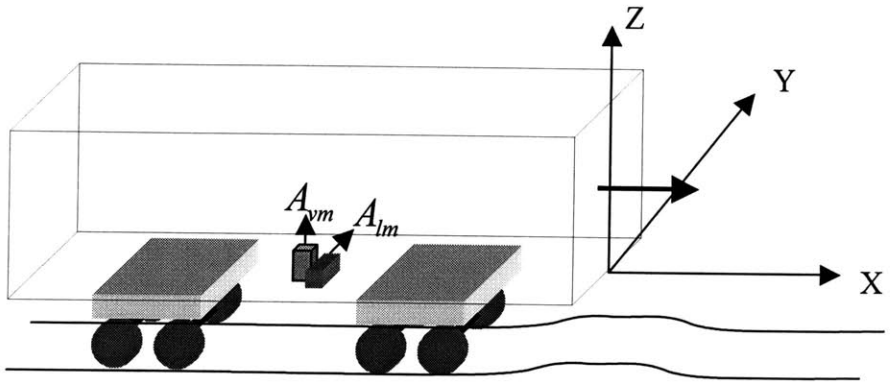

(a) Two Accelerometers in the Middle of the Vehicle's Floor

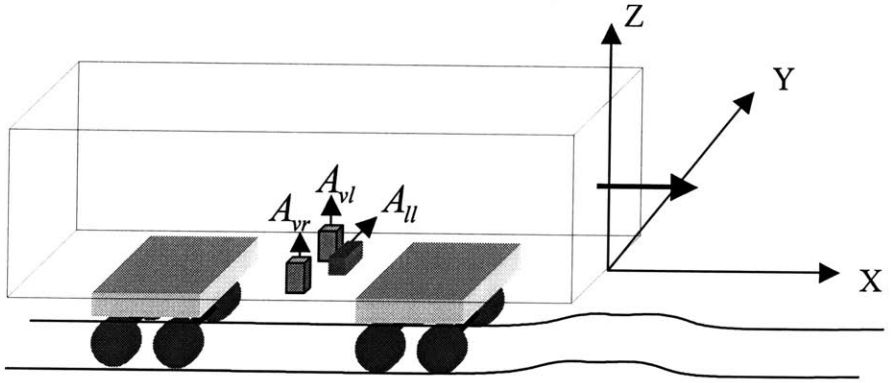

(b) Three Accelerometers in the Middle of the Vehicle's Floor

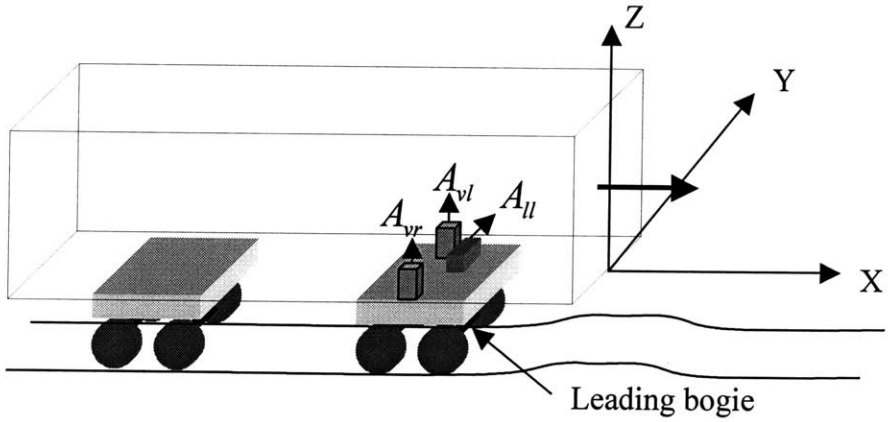

(c) Three Accelerometers over the Leading Bogie

Figure 3.5 Positions of the Accelerometers

Figure 3.6 details how we identify an inverse model. First, in the original model, three types of irregularities and three accelerations are selected as inputs so that each input corresponds to each output. While lateral and vertical accelerations (A_{ll} and A_{vl}) on the left side of the car correspond to Lateral Irregularities (I_{ll}) and Vertical Irregularities (I_{vl}) respectively, the difference between the vertical accelerations on the left side and on the right side ($A_{vr} - A_{vl}$) is associated with Level Irregularities (I_e).

As a result, the inverse system can be modeled as a three-input and three-output MIMO system.

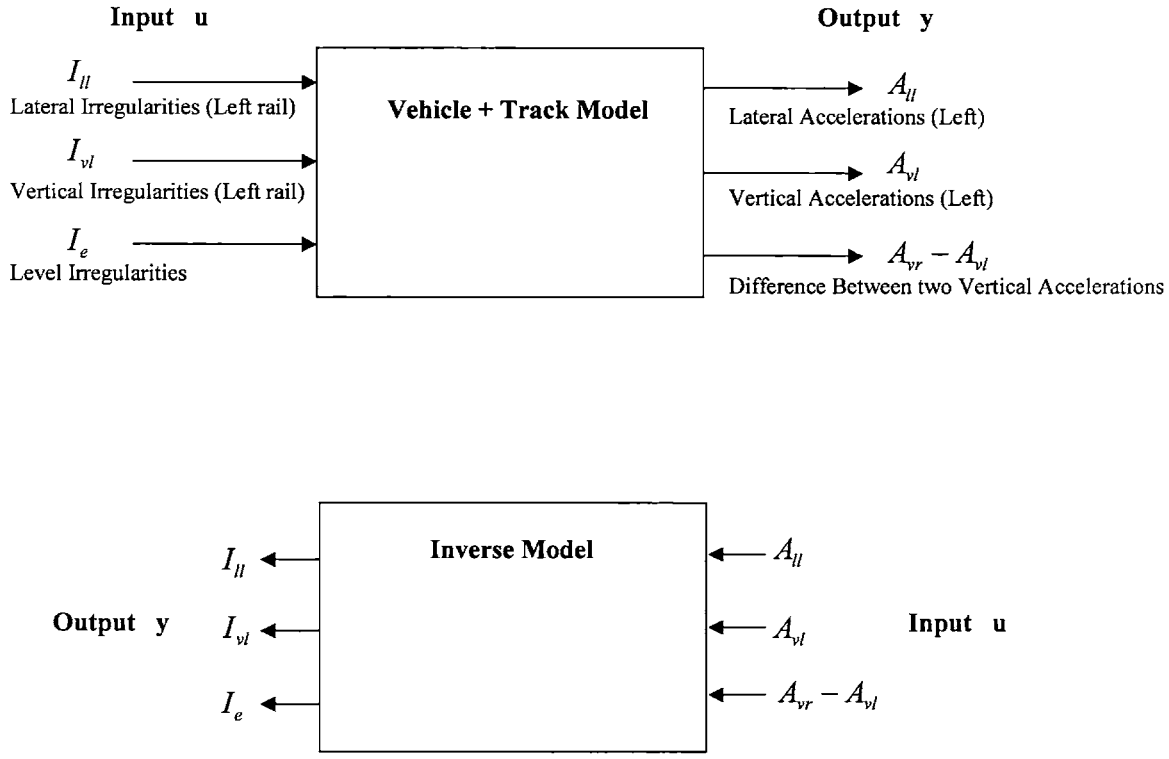

Figure 3.6 An Inverse System

The ARX model for the MIMO system can be described as,

$$\mathbf{y}(t)+\mathbf{C}_1\mathbf{y}(t-1)+\ldots+\mathbf{C}_n\mathbf{y}(t-n)=\mathbf{D}_1\mathbf{u}(t)+\mathbf{D}_2\mathbf{u}(t-1)+\ldots+\mathbf{D}_m\mathbf{u}(t-m+1)+\mathbf{e}(t) \quad (3.9)$$

where

$$\mathbf{y}(t)=\begin{bmatrix} I_{ll}(t) \\ I_{vl}(t) \\ Ie(t) \end{bmatrix},$$

$$\mathbf{u}(t)=\begin{bmatrix} A_{ll}(t) \\ A_{vl}(t) \\ A_{vr}-A_{vl}(t) \end{bmatrix},$$

$\mathbf{C}_1\ldots\mathbf{C}_n$ and $\mathbf{D}_1\ldots\mathbf{D}_m$ are 3×3 parameter matrices, and

$\mathbf{e}(t)$ is a 3×1 disturbance vector.

Equation (3.9) can be expressed as,

$$\mathbf{A}(q)\mathbf{y}(t)=\mathbf{B}(q)\mathbf{u}(t-k)+\mathbf{e}(t) \quad (3.10)$$

where

$\mathbf{A}(q)=\mathbf{I}+\mathbf{C}_1q^{-1}+\ldots.+\mathbf{C}_nq^{-n}$,

$\mathbf{B}(q)=\mathbf{D}_1+\mathbf{D}_2q^{-1}+\ldots+\mathbf{D}_mq^{-m+1}$, and

k is the number of delays from input to output.

Figure 3.7 shows the model construction period and the model validation period. At the first attempt, we select 4000 meters were used for the model construction. The results of the estimation were not good, because 4000 meters are not enough to excite the system sufficiently. Thus, we select 8000 meters for the model construction period. The last 2000 meters will be used for the model validation.

To obtain the parameter vector estimate $\hat{\theta}_N$, $\sum_{i=1}^{N}\varphi(i)\varphi^T(i)$ in Equation (3.8) must be invertible. To ensure this, inputs must excite sufficiently outputs. For example, some of the left vertical irregularities are outside the standard range in Figure 3.7 and excite the system sufficiently. Therefore, vertical accelerations sufficiently excite the left vertical irregularity for an inverse model. Although we need 8000 meters for the model construction, we do not need such a long distance data if inputs sufficiently excite the outputs.

The next two sections describe the model construction and the model validation.

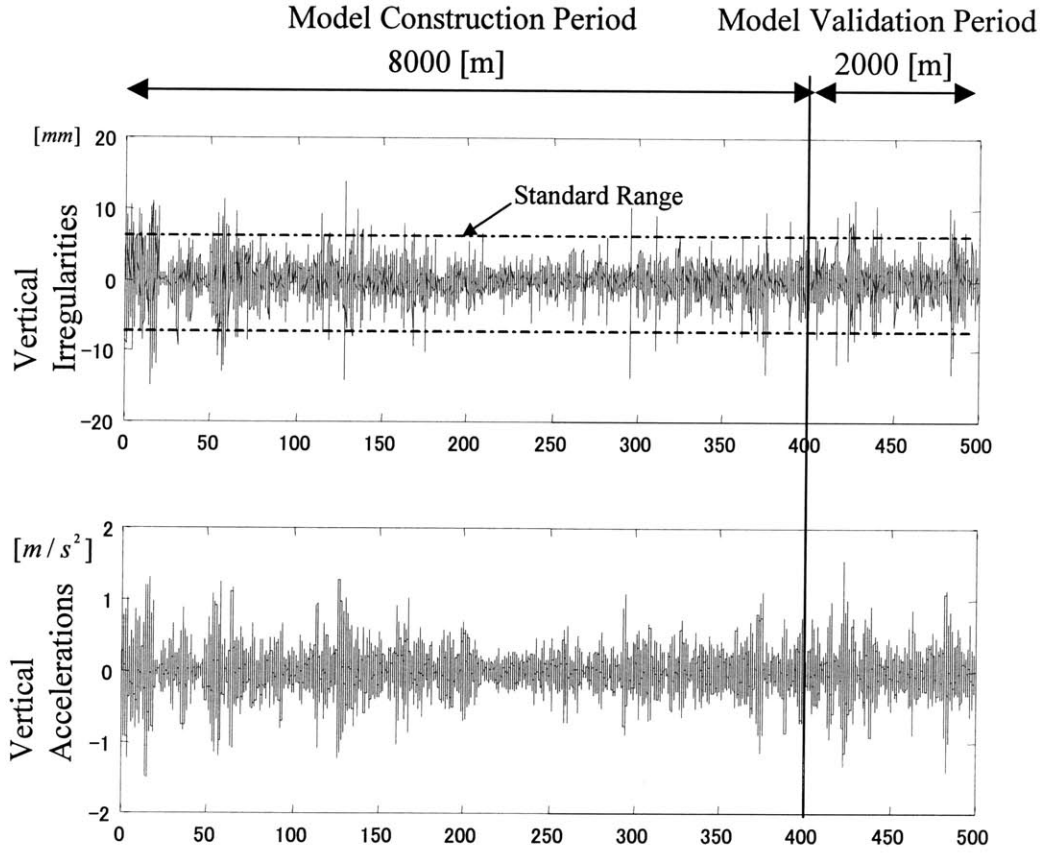

Figure 3.7 A Model Construction Period and a Model Validation Period

3.3 Model Construction

3.3.1 Results of Model Construction

Based on the inverse model in Fig.3.5, the input is expressed as

$$\mathbf{u}(t) = \begin{bmatrix} A_{ll}(t) \\ A_{vl}(t) \\ A_{vr} - A_{vl}(t) \end{bmatrix},$$

and the output is expressed as

$$\mathbf{y}(t) = \begin{bmatrix} I_{ll}(t) \\ I_{vl}(t) \\ Ie(t) \end{bmatrix}.$$

The data of the irregularity for the model construction period in Figure 3.6 are given every 1 meter in the simulations. In practice, waves of 25-meter lengths, which come from the length of a rail, are dominant in rail irregularities, and an inspection car practically measures the rail irregularity every 1 meter [11]. The irregularity data are given every 1 meter, which is enough to represent 25-meter waves of the irregularity.

The data for the input $\mathbf{u}(t)$ and $\mathbf{y}(t)$ in the model construction period are used to obtain parameters in $\mathbf{A}(q)$ and $\mathbf{B}(q)$ of Equation (3.10). Equation (3.8) is used to obtain $\hat{\theta}_N$, which minimizes V_N in Equation (3.7).

Table 3.2 shows the obtained model orders. Because orders of the model structure can be infinite, these were obtained by trial and error so that the order was made as low as possible. First, the maximum number of the order is selected. Next, the mean square error for the predicted for the model construction period is calculated for all the

models up to the selected maximum order. The high the order is, the smaller the mean square error is. However, the decrease of the mean square saturates at a certain order, which is selected as the order of the model. Appendix C shows the Transfer Function of the model.

Table 3.2 Orders of the ARX model

Output: n	Input: m	Delay: k
10	10	1

Figure 3.8 shows the actual Left Lateral Irregularity (I_{ll}) and the predicted Left Lateral Irregularity ($\hat{I}_{ll}$) by using the resulting model for the entire model construction period. The corresponding error ($I_{ll} - \hat{I}_{ll}$) is shown in Figure 3.9. The acceptable range is based on Table 2.1. Some peaks of error are outside the acceptable range, because there is a small gap in phase between the actual irregularity and the predicted irregularity, which is shown in Figure 3.10. Figure 3.10 presents a comparison between the actual Left Lateral Irregularity and its corresponding predicted irregularity for the range from 120 [sec] to 130 [sec]. Although Figure 3.10 shows a good agreement in magnitude, there is a small gap in phase at the peak where time is 125 [sec]. The gap equals to 0.2 [sec]. Since the speed of a vehicle is 20 [m/sec], the gap equals to 4 [m]. From a practical point of view, the gap of 4 [m] is acceptable for the maintenance work, when we can find a rail that has unacceptable irregularity by the magnitude.

In the same manner, Figures 3.11 and 3.12 present results of the Vertical Irregularity and Figures 3.13 and 3.14 present results of the Level Irregularity. As for the Vertical Irregularity, Figure 3.12 shows that the predicted irregularity agree well in both

magnitude and phase. However, in Figure 3.15 for the Level Irregularity, the model has a good agreement in phase, while performance for magnitude is not acceptable.

We must consider the reason that we have error in predicted irregularities, although we construct a model with known inputs and outputs. We use the ARX Model that is described as Equation (3.3), which is based on the assumption that there is a linear relationship between inputs and outputs. However, as explained in Chapter 2, we have many non-linear components in the vehicle's suspensions. The Error for the Lateral Irregularity is larger than that for the Vertical Irregularity, because the effects of non-linear components are larger in the lateral direction than in the vertical direction. As for the error of Level Irregularity, the estimate does not agree well with the actual irregularity, especially in magnitude. The locations and the number of accelerometers should be studied.

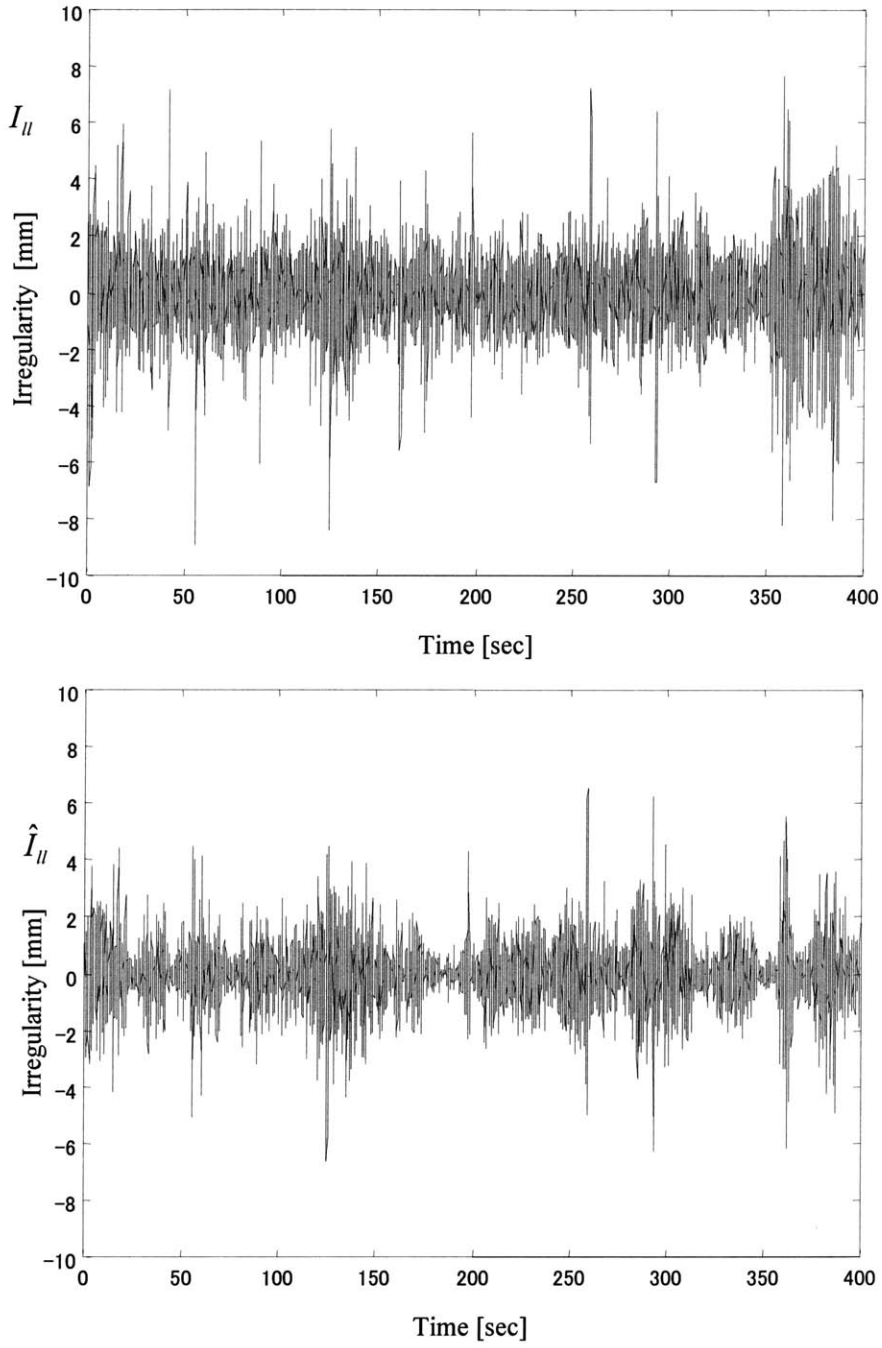

Figure 3.8 Actual Left Lateral Irregularity (Top) and Predicted Left Lateral Irregularity (Bottom)

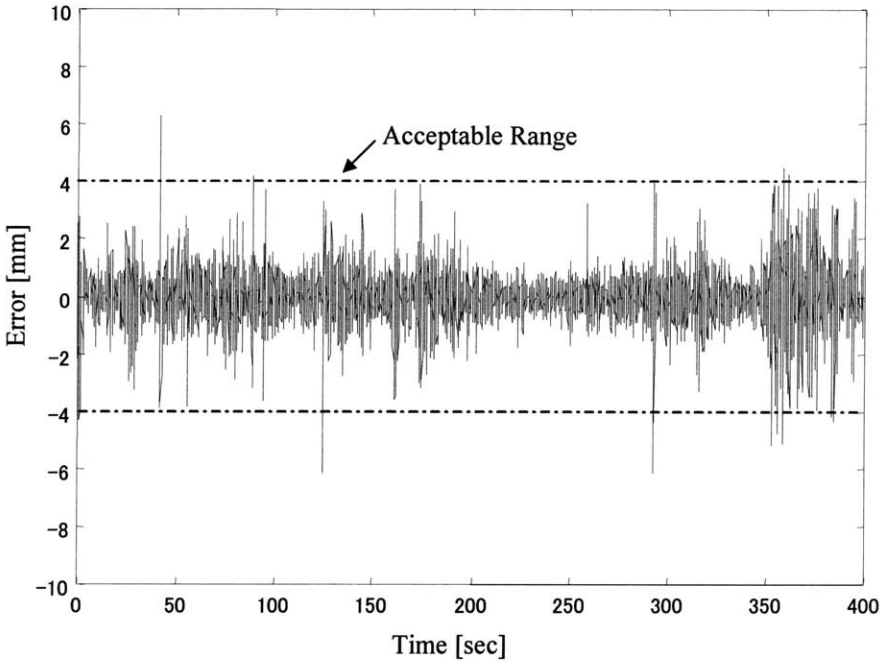

Figure 3.9 Error between the Actual Left Lateral Irregularity and the Predicted Left Lateral Irregularity ($I_{ll} - \hat{I}_{ll}$)

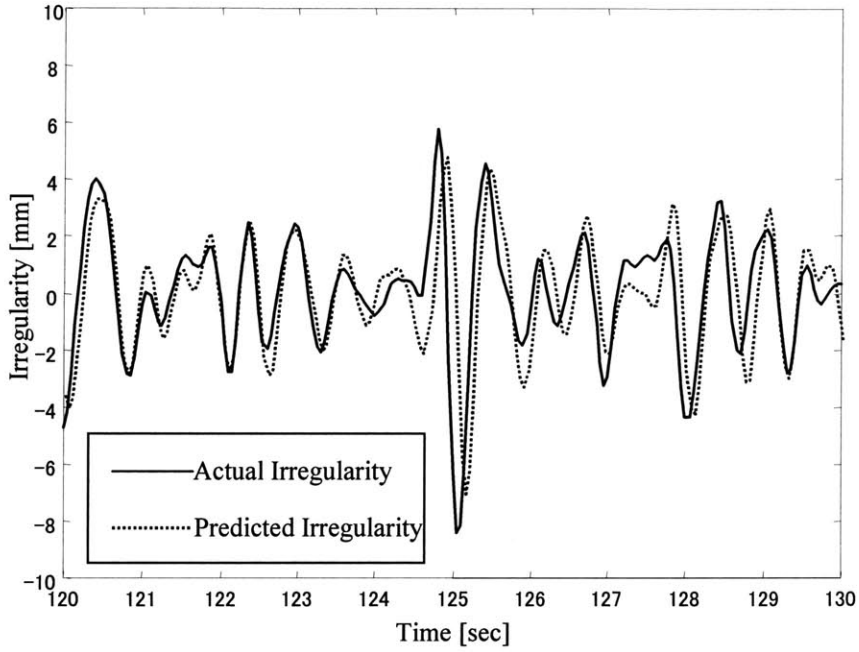

Figure 3.10 Actual Left Lateral Irregularity vs. Predicted Left Lateral Irregularity

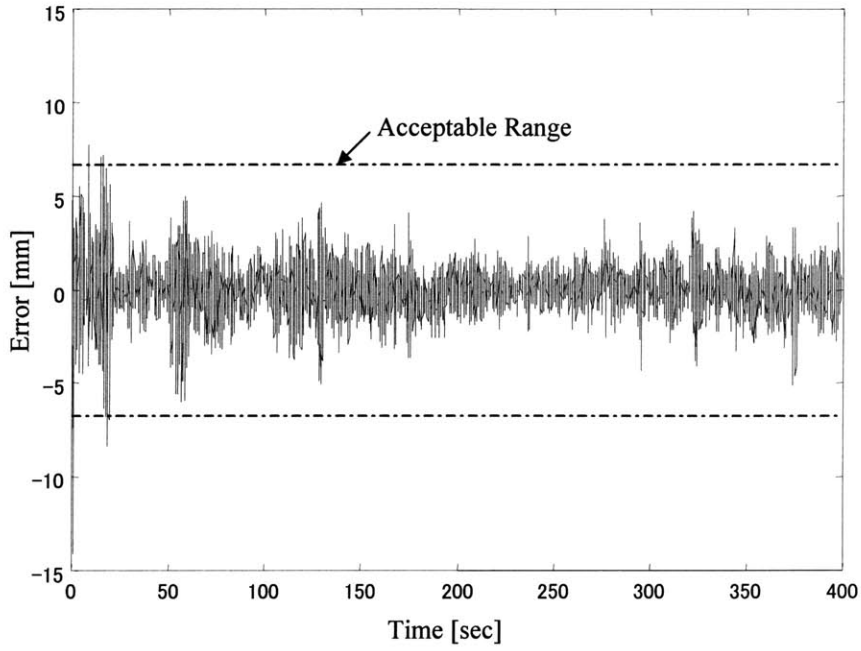

Figure 3.11 Error between the Actual Left Vertical Irregularity and the Predicted Left Vertical Irregularity ($I_{vl} - \hat{I}_{vl}$)

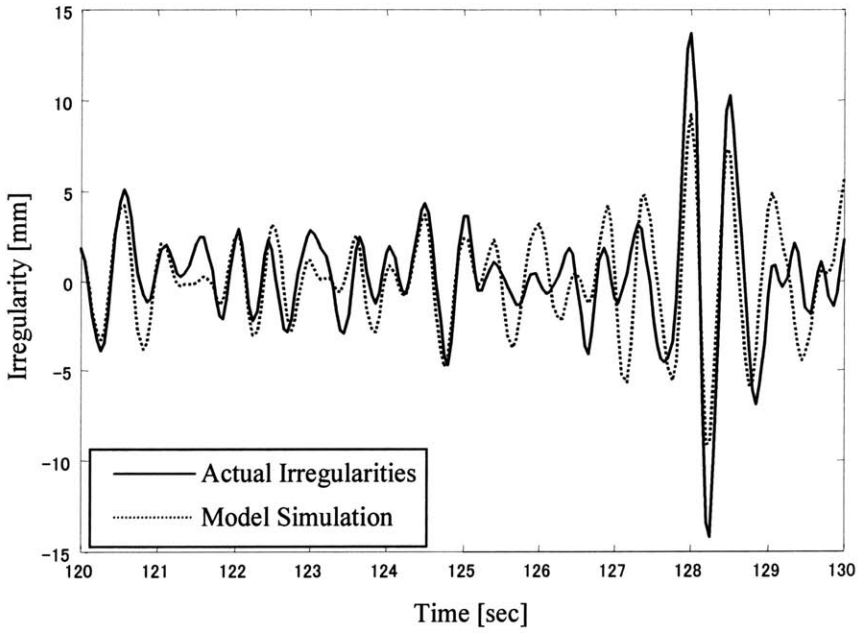

Figure 3.12 Actual Left Vertical Irregularity vs. Predicted Left Vertical Irregularity

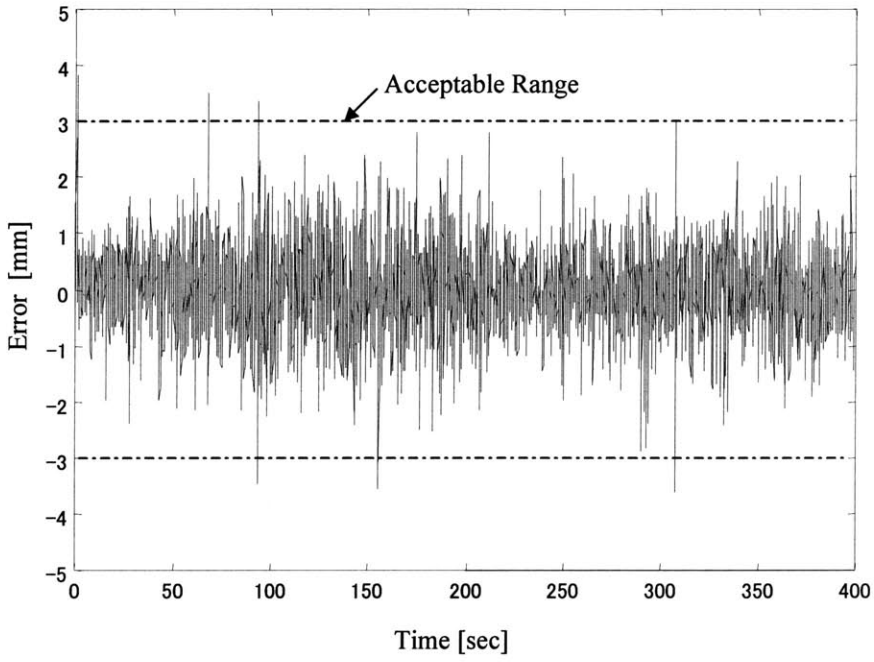

Figure 3.13 Error between the Actual Level Irregularity and the Predicted Level Irregularity ($I_e - \hat{I}_e$)

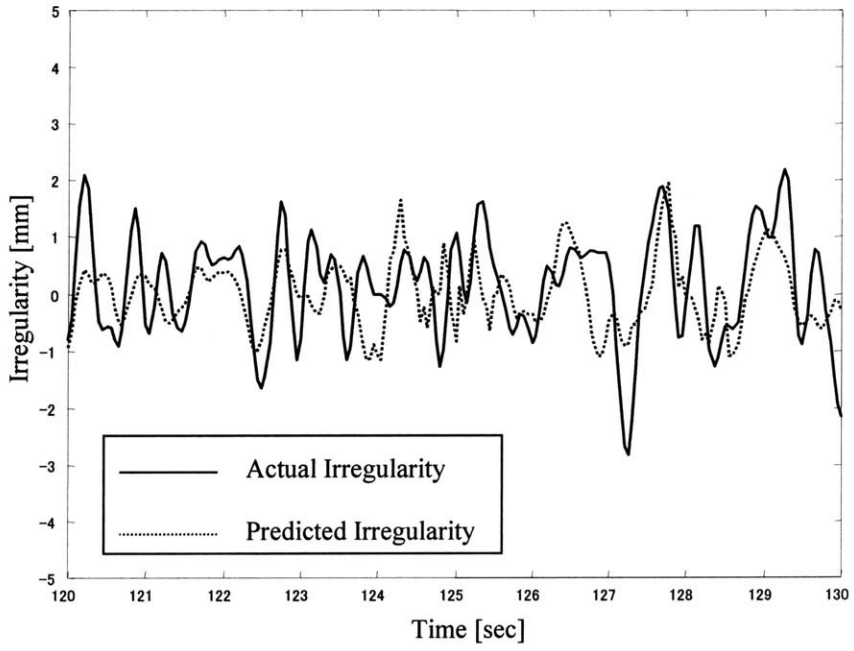

Figure 3.14 Actual Level Irregularity vs. Predicted Level Irregularity

3.3.2 A Practical Issue for Model Construction

In practice, we cannot use the inverse model obtained by the simulation to estimate the actual irregularity, because the properties of an actual vehicle differ from those of a modeled vehicle in the simulation. Therefore, we must consider how to construct an inverse model in practice.

We can measure the actual rail irregularity by using a conventional inspection car. After obtaining data of accelerations by making a vehicle run on the rail, we can use the same technique as this section to identify an inverse model.

When we locate the rail whose irregularities are outside the standard range, maintenance workers manually measure the rail irregularity before aligning rails. Therefore, we can obtain known irregularities and accelerations from this location. We can calibrate and update the model by using these data.

3.4 Model Validation

3.4.1 Results of Validation

In order to validate the model obtained in Section 3.2, estimates generated by the model are evaluated using irregularity data that were not used for constructing the model.

Figures 3.15 and 3.16 show, respectively, error between the actual Left Lateral Irregularity and its corresponding estimate, and the actual Left Lateral Irregularity and its corresponding estimate for the range from 430 [sec] to 440 [sec]. Some peaks of the error are outside the acceptable range, since there are small phase gaps at the peaks, as shown in Figure 3.16. This gap equals to 4 [meter], as explained in Subsection 3.3.1. From a practical point of view, the gap of 4 [m] is acceptable.

Figures 3.17 and 3.18 show, respectively, error between the actual Left Vertical Irregularity and its corresponding estimate, and the actual Left Vertical Irregularity and its corresponding estimate for the range from 430 [sec] to 440 [sec]. Figure 3.17 shows error is acceptable. Figure 3.18 shows that the estimate agrees well with the actual irregularity in both phase and magnitude at the peak where time is 439.5 [sec].

Figures 3.19 and 3.20 show, respectively, error between the actual Level Irregularity and its corresponding estimate, and the actual Level Irregularity and its corresponding estimate for the range from 430 [sec] to 440 [sec]. Some peaks of the error are outside the acceptable range, since estimate does not agree well with the actual irregularity, as shown in Figure 3.20.

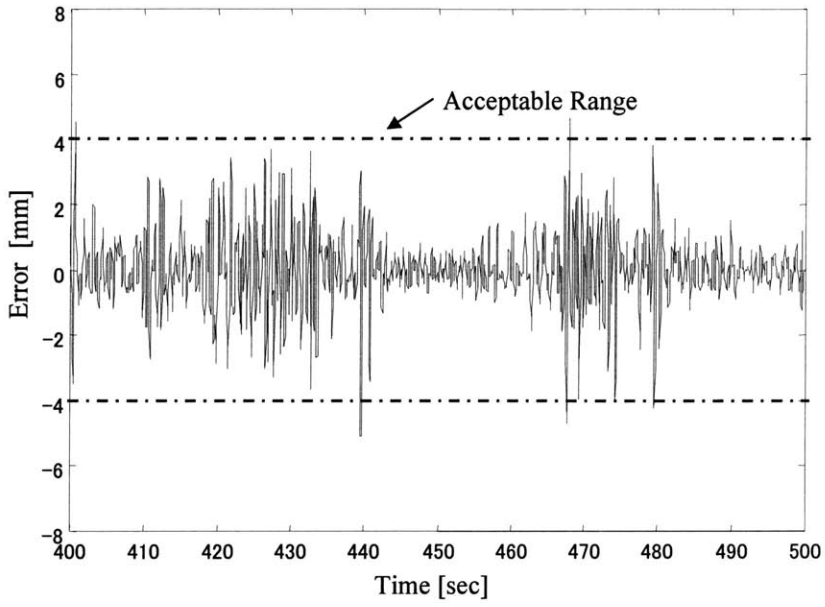

Figure 3.15 Left Lateral Irregularity: Error ($I_{ll} - \hat{I}_{ll}$)

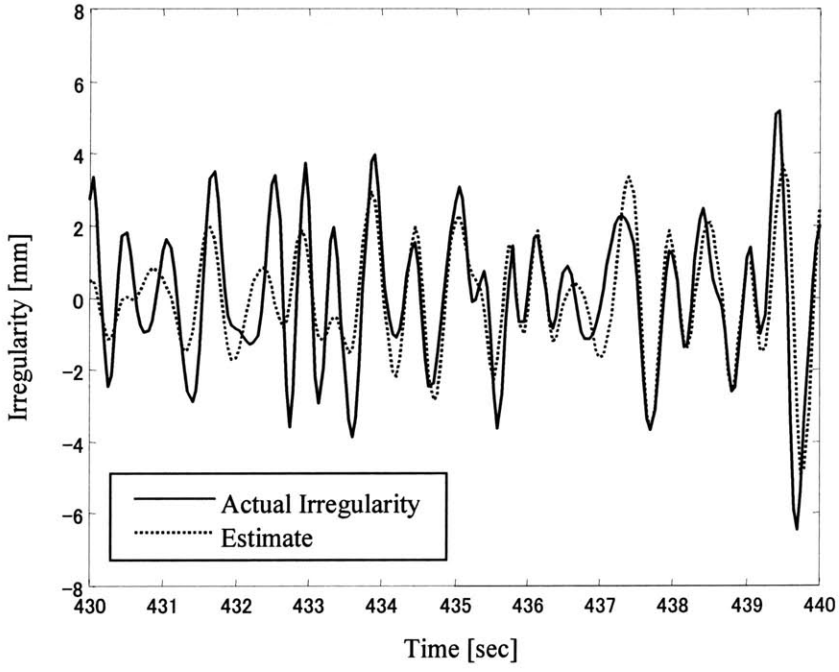

Figure 3.16 Left Lateral Irregularity: Actual (I_{ll}) and Estimate ($\hat{I}_{ll}$)

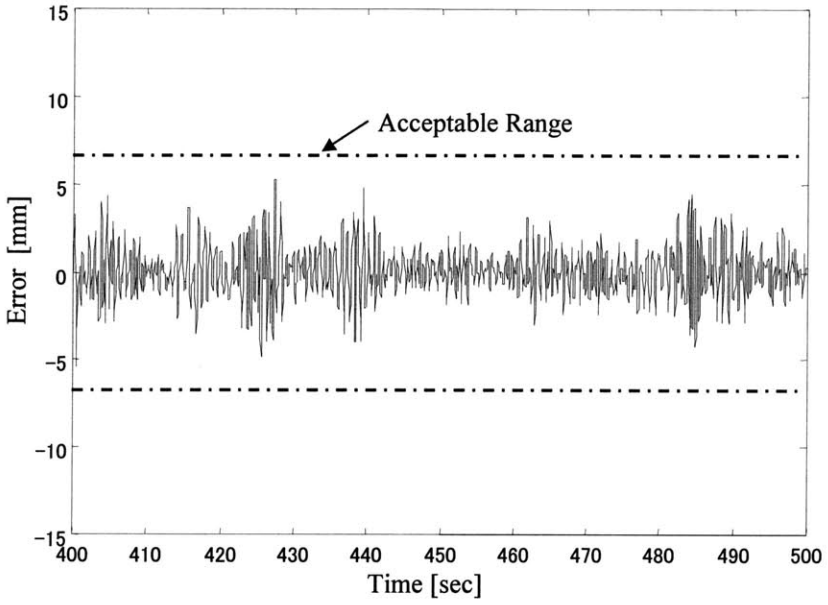

Figure 3.17 Left Vertical Irregularity: Error ($I_{vl} - \hat{I}_{vl}$)

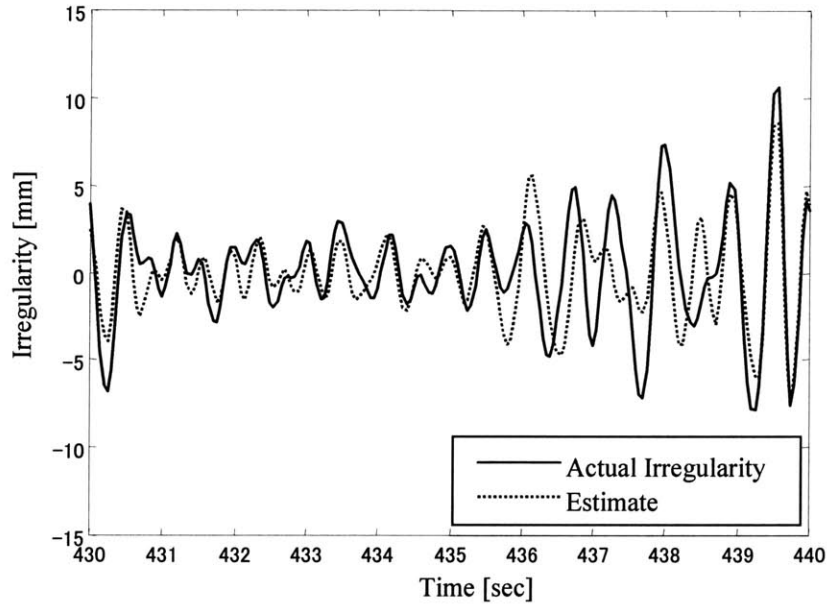

Figure 3.18 Left Vertical Irregularity: Actual (I_{vl}) and Estimate ($\hat{I}_{vl}$)

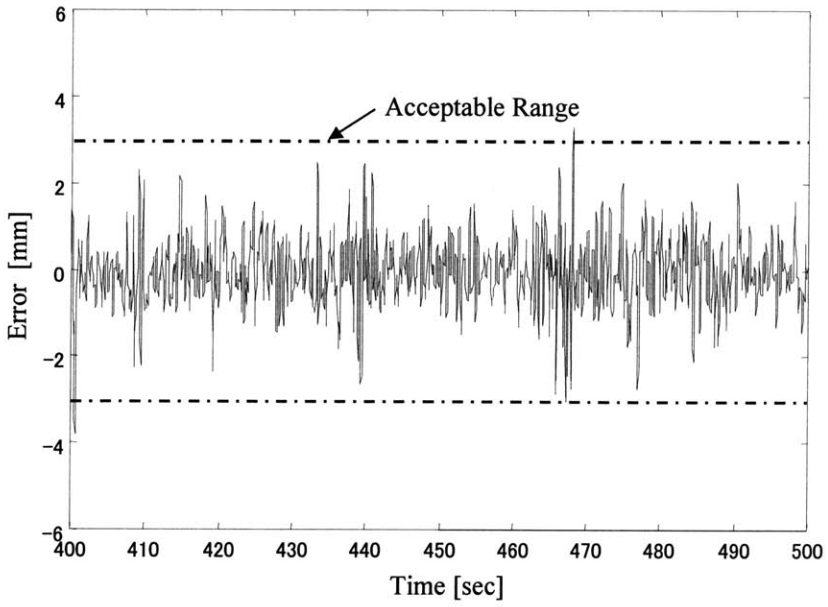

Figure 3.19 Level Irregularity: Error ($I_e - \hat{I}_e$)

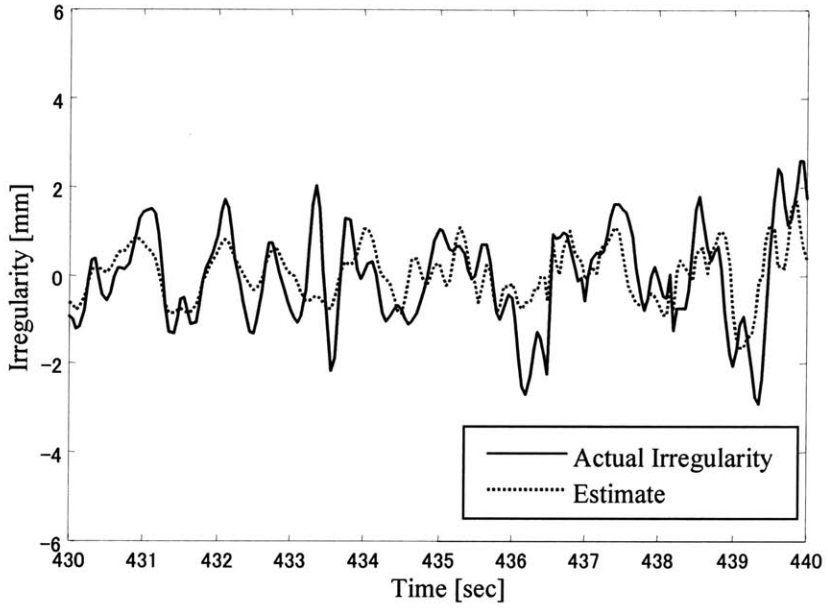

Figure 3.20 Level Irregularity: Actual (I_e) and Estimate ($\hat{I}_e$)

3.4.2 Evaluation by the Mean Square Error

The Mean Square Error (MSE) is a general method of evaluating errors:

$$MSE = \sqrt{\frac{\sum_{k=1}^{N} (y(k) - y_e(k))^2}{N}}.$$

where

N is the number of data,

$y(k)$ is an actual irregularity to be obtained, and

$y_e(k)$ is an estimated irregularity.

Table 3.3 shows the MSE values for the resulting model and model validation. The simulations were executed under the conditions shown in Table 3.1. The results in Figures 3.18, 3.11, and 3.14 are used to compute the MSE values for the resulting model. The results in Figures 3.17, 3.20, and 3.23 are used for the MSE values for model validation.

As shown in Figures 3.18, 3.11, and 3.14, and Table 3.3, there are errors in the estimates. This is because the system has non-linear properties. The MSE values for the resulting model are limitations in estimates produced by the ARX model.

Table 3.3 MSE for Model Simulation and Validation

Types of Irregularities	MSE for Resulting Model	MSE for Validation
Lateral Irregularities	0.948	1.070
Vertical Irregularities	1.336	1.336
Level Irregularities	0.718	0.761

Although the MSE values for Level Irregularities are smaller than others in Table 3.3, this does not necessarily mean that estimates for Level Irregularities are the best of all. Since the entire range for each irregularity differs, the range should be included in the assessment. Table 3.4 shows the upper and lower limits for each irregularity.

The MSE values can be considered as absolute values of average errors in estimates. The resolution is the minimum value that can be discerned by the estimation. Since the actual irregularity is within the range of the estimate ± MSE value, the resolution can be considered as twice as much as MSE value:

$$\text{Resolution} = 2 \times MSE$$

The third column of table 3.4 shows the resolutions for irregularities, which are twice as much as the second column of Table 3.5. In order to compare the resolutions for irregularities, we define the resolving power in the following equation:

$$\text{Resolving Power} = \frac{\text{Total Range of the Irreuglarity}}{\text{Resolution}}.$$

The forth column of Table 3.4 shows the resolving powers for the irregularities. For example, for the Lateral Irregularity, the ratio of the total range for the resolution of the estimation is 9.494. Contrary to the MSE value, the resolving power for Vertical Irregularities is the highest of all, followed by that for Lateral Irregularities. This means that estimation for the Vertical Irregularity has the finest scale for the total range.

Table 3.4 Resolutions of the Estimation

Types of Irregularities	Upper and Lower Limits	Total Range	Resolution	Resolving Power
Lateral Irregularities	±9 [mm]	18 [mm]	1.896	9.494
Vertical Irregularities	±15 [mm]	30 [mm]	2.672	11.228
Level Irregularities	±5 [mm]	10 [mm]	1.436	6.964

3.4.3 Evaluation by the Warning Test

From a practical point of view, the main objective of estimation is to locate rails whose irregularities go over the limit rather than to obtain the accurate values of irregularities throughout a section. As mentioned in Chapter 2, we have a standard value for each type of irregularity for maintenance work. If a measurement goes over the standard value, alignment of rails must be done.

Therefore, this project introduces a warning system that provides us with warnings when estimates go over a certain value. In Table 3.5, thresholds for three types of irregularities are selected and Figure 3.25 shows an example of warnings for the Vertical Irregularities. As shown in Figure 3.25, 0.25-sec time slots are set and either a warning or no warning is given in each slot according to the estimates in the slot. Thus, the total number of warnings is 400 times in 100 [sec] of total period of validation.

Table 3.5 Thresholds for Warnings

Types of Irregularity	Thresholds
Lateral	±3 [mm]
Vertical	±5 [mm]
Level	±1 [mm]

Rules of the warning system are outlined as follows:

1) If one of the estimates in a slot goes over a threshold, a warning for an abnormal irregularity is given.

1-1) If the corresponding actual irregularity is abnormal, the warning is considered a correct warning.

1-2) If the corresponding actual irregularity is normal, the warning is incorrect. This error is referred to as a *Type 1 Error*.

2) If one of the estimates in a slot does not go over a threshold, a warning for an abnormal irregularity is not given.

2-1) If the corresponding actual irregularity is normal, the warning system is correct.

2-2) If the corresponding actual irregularity is abnormal, the warning system fails to work. This is referred to as a *Type 2 Error*. Obviously, we should avoid Type 2 Errors rather than Type 1 Errors for safety.

In addition, the lower the number of total warnings is, the more reliable a warning system is.

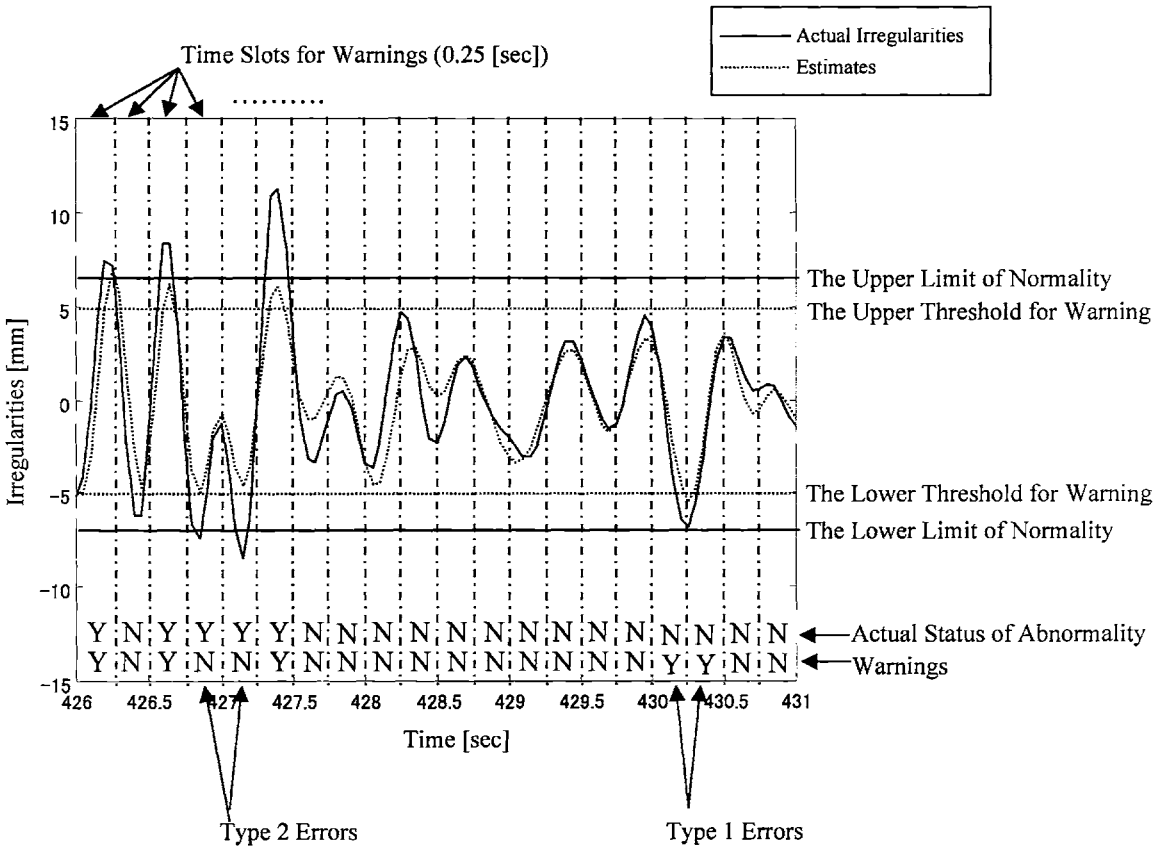

Figure 3.21 An Example of a Warning Test

The results of warning tests are shown in Tables 3.6, 3.7 and 3.8. The results of warning tests depend on the setting of warning thresholds. The Type 1 Errors increase and the Type 2 Errors decrease if the thresholds are low. On the other hand, if the thresholds are high, the Type 1 Errors decrease and the Type 2 Errors increase. Therefore, the thresholds in Table 3.5 are selected so that the rates of the Type 2 Error are less than 2 %. Type 1 Errors are less than 20% and Type 2 Errors are less than 2% for the Lateral Irregularities and the Vertical Irregularities. These results seem that the

warnings for the Lateral Irregularities and the Vertical Irregularities are reliable. However, the implementation of these estimations depends on whether Type 1 Errors and Type 2 Errors are acceptable for a practical management of maintenance work. To find out the optimal thresholds for Type 1 Errors and Type 2 Errors is needed for the improvement of the results.

While reliabilities for warnings are more than 80 % in both Lateral Irregularities (81.8 %) and Vertical Irregularities (85.7 %), reliability for warnings is 43.2 % in Level Irregularities. This is because the estimation for Level Irregularities does not agree well in magnitude, as shown in Figures 3.15 and 3.24. This means that we have to improve the location and the number of accelerometers to detect Level Irregularities.

Table 3.6 Results of Warning Test for Lateral Irregularities

		Warning by Estimation	
		No Warning	Warning
Actual Lateral Rail Irregularity	Normal	371 (times)	4 (times)
		98.1 (%)	18.2 (%)
	Abnormal	7 (times)	18 (times)
		1.9 (%)	81.8 (%)
Subtotal		378 (times)	22 (times)
		94.5 (%)	5.5 (%)
Total		400 (times)	

Table 3.7 Results of Warning Test for Vertical Irregularities

		Warning by Estimation	
		No Warning	Warning
Actual Vertical Rail Irregularity	Normal	369 (times)	4 (times)
		99.2 (%)	14.2 (%)
	Abnormal	3 (times)	24 (times)
		0.8 (%)	85.7 (%)
Subtotal		372 (times)	28 (times)
		93 (%)	7 (%)
Total		400 (times)	

Table 3.8 Results of Warning Test for Level Irregularities

		Warning by Estimation	
		No Warning	Warning
Actual Vertical Rail Irregularity	Normal	358 (times)	21 (times)
		98.6 (%)	56.7 (%)
	Abnormal	5 (times)	16 (times)
		1.4 (%)	43.2 (%)
Subtotal		363 (times)	37 (times)
		92.5 (%)	7.5 (%)
Total		400 (times)	

3.5 Summary

A method for estimating rail irregularities is proposed. A MIMO system is presented to identify an inverse system whose inputs are accelerations and outputs are irregularities. The ARX model for the MIMO system is obtained by using simulation data. To validate the resulting ARX model, resolutions of estimation are presented. In addition, a warning test for practical maintenance work is proposed. Both results show that estimates for the Vertical Irregularities agree well with actual irregularities.

We consider the reason that we have error in predicted irregularities. We use the ARX Model that is described as Equation (3.3), which is based on the assumption that there is a linear relationship between inputs and outputs. However, as explained in Chapter 2, we have some non-linear components in the vehicle's suspensions. Therefore, non-linear components can be considered one of the reasons for the error. Another reason is the location of the accelerometers. In particular, as for the Level Irregularity, the estimate does not agree well with the actual irregularity. The locations and the number of accelerometers should be studied.

4 Assessment of Practical Implementation

4.1 Introduction

Chapter 3 considered the system with no uncertainty. However, in practice, various uncertainties exist. In this study, we consider two major. One is mass variation due to the change of the weight of a passenger car at each station. The other is speed variation, which may change at any time. Section 4.2 assesses effects of these uncertainties by using Singular Value Plots. Section 4.3 proposes a compensation method for these effects.

4.2 Effects of System Uncertainties

4.2.1 Mass Variation

Chapter 3 presented how accurately we can estimate irregularities if we do not have any uncertainties. We must assess how the model with uncertainties. First, this subsection assesses mass variation.

Generally, two types of uncertainty models are used when we deal with unstructured uncertainties. Figure 4.1 shows the Additive Uncertainty and the Multiplicative Uncertainty. The Multiplicative Uncertainty has an advantage over the Additive Uncertainty when we design a controller for a plant [17]. However, this methodology does not involve any controllers. In addition, while the Multiplicative

Uncertainty covers unmodeled high-frequency dynamics of sensors and actuators, the Additive Uncertainty treats additive plant errors. Since the mass variation and the speed variation can be considered additive plant errors, we select the Additive Uncertainty. The effects of the uncertainties are expressed as

$$\Delta(s) = G_a(s) - G(s) \tag{4.1}$$

where

$G_a(s)$ is the transfer function of an actual continuous model with an uncertainty from mass variation or speed variation and $G(s)$ is the transfer function of a nominal model without uncertainties.

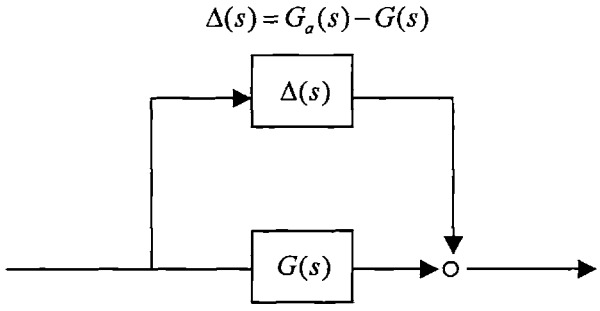

Additive Uncertainty

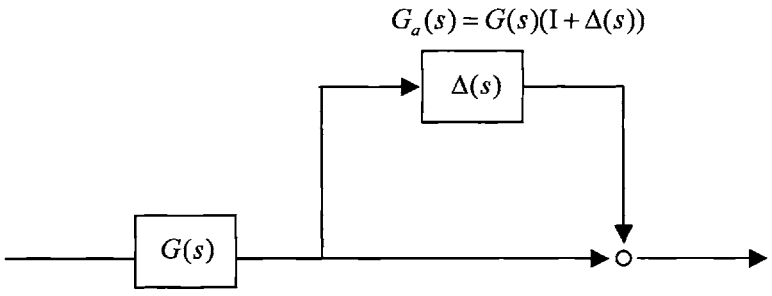

Multiplicative Uncertainty

Figure 4.1 Uncertainty Models

While the Bode Plot is used to obtain frequency responses for SISO systems, the Singular Value Plot can play a similar role for MIMO systems. We have a discrete three-input and three-output MIMO system expressed as

$$\mathbf{Y}(z) = \mathbf{G}(z)\mathbf{U}(z)$$

where

$\mathbf{Y}(z)$ is the Z Transform of $\mathbf{y}(t) = \begin{bmatrix} I_{ll}(t) \\ I_{vl}(t) \\ Ie(t) \end{bmatrix}$ and

$\mathbf{U}(z)$ is the Z Transform of $\mathbf{u}(t) = \begin{bmatrix} A_{ll}(t) \\ A_{vl}(t) \\ A_{vr} - A_{vl}(t) \end{bmatrix}$.

The Singular Value Decomposition at the frequency w for $\mathbf{G}(z)$ is:

$$\mathbf{G}(e^{jw}) = U\Sigma V^* = \begin{bmatrix} U_{\max} & U_2 & U_{\min} \end{bmatrix} \begin{bmatrix} \sigma_{\max} & 0 & 0 \\ 0 & \sigma_2 & 0 \\ 0 & 0 & \sigma_{\min} \end{bmatrix} \begin{bmatrix} V_{\max} & V_2 & V_{\min} \end{bmatrix}^* \quad (4.2)$$

where

$U_{\max}, U_2, U_{\min}, V_{\max}, V_2$, and $V_{\min}$ are 3×1 vectors, and the operator $*$ indicates the transpose and complex conjugate. The vector $V_{\max}$ is the direction where output $\mathbf{y}$ has the maximum magnitude, $\|\mathbf{y}\|_2 = \|\sigma_{\max} U_{\max}\|_2 = \sigma_{\max}$ and $V_{\min}$ is the direction where output has the minimum magnitude, $\|\mathbf{y}\|_2 = \|\sigma_{\min} U_{\min}\|_2 = \sigma_{\min}$.

Before computing the Singular Values for uncertainty models, we consider the range of inputs. If we can show a certain range is dominant in inputs, we do not compute

the Singular Values along the all frequencies. Figures 4.2 and 4.3 present the Fourier Transforms of input signals. While the frequencies from 0.9 [Hz] to 1.85 [Hz] are dominant for the lateral accelerations, the range from 1.35 [Hz] to 1.80 [Hz] is main for the vertical accelerations. Since the range for the lateral accelerations includes the range for the vertical accelerations, the range for the lateral accelerations will be the range of interest for Singular Value Plots.

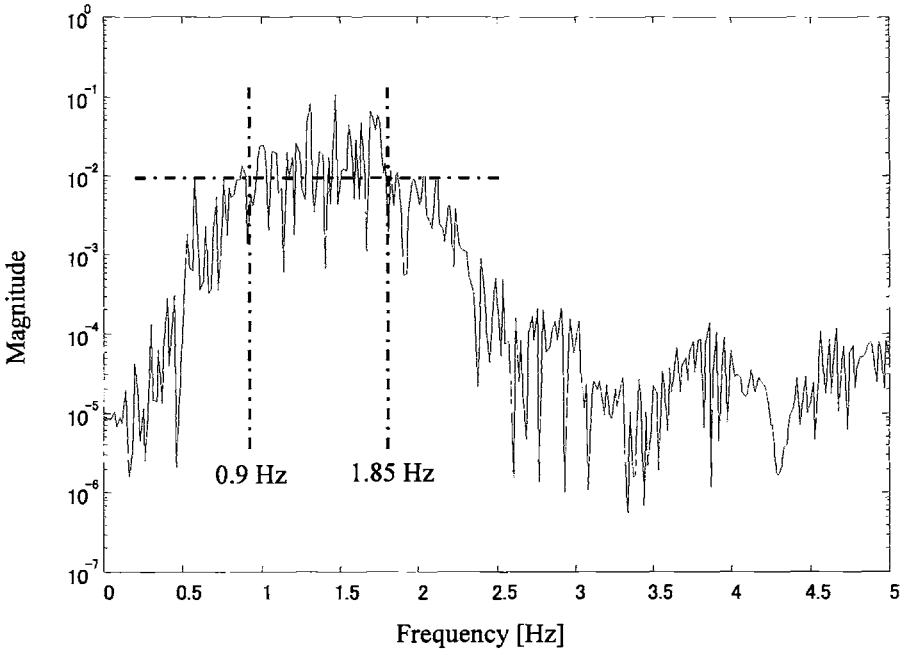

Figure 4.2 FFT of Lateral Accelerations

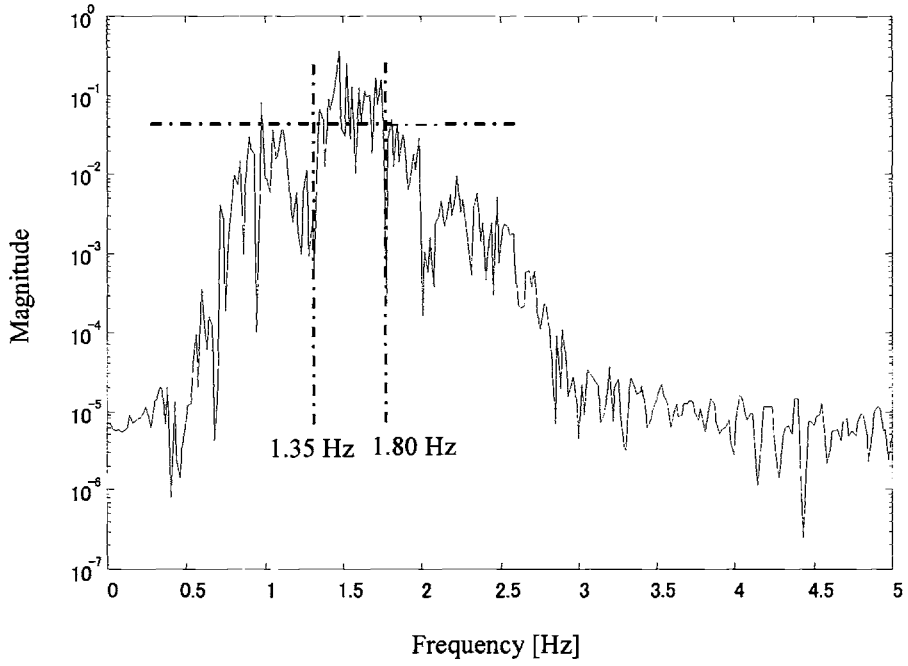

Figure 4.3 FFT of Vertical Accelerations

In Chapter 3, we obtained $\mathbf{G}(z)$ for the model, which is described in Appendix C. Equation (4.1) for a continuous system can be expressed as

$$\Delta(z) = \mathbf{G}_a(z) - \mathbf{G}(z) \tag{4.3}$$

for a discrete MIMO system. Figure 4.4 shows the Singular Value Plot for the nominal model $\mathbf{G}(z)$ in which the mass is 52,000 [kg] and $\Delta(z)$ where $\mathbf{G}_a(z)$ has a 1% increase (520 [kg]) of a vehicle's mass. 520 [kg] is the mass of 7 passengers. Figure 4.4 indicates that the uncertainty model $\Delta(z)$ attenuates most of the input signals in the range of interest, compared to the nominal model. Outputs that are magnified by the uncertainty model $\Delta(z)$ seem to be much smaller than outputs from the nominal model.

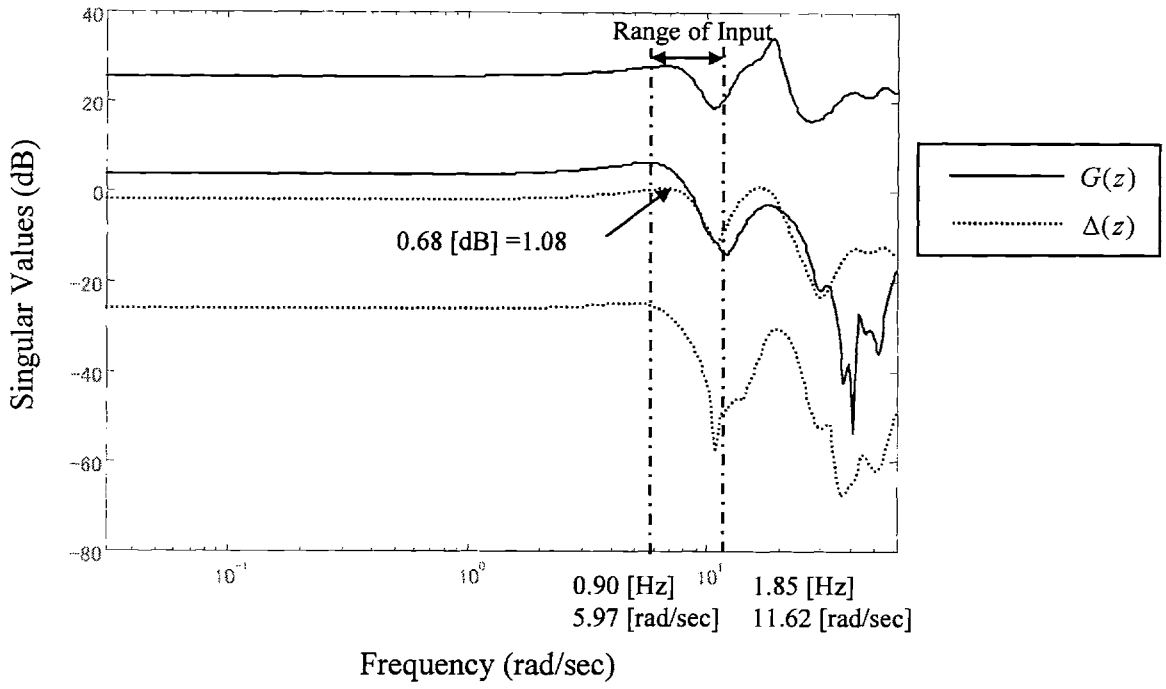

Figure 4.4 Singular Value Plots for a Nominal Model (Mass = 52000 [kg]) $G(z)$ and an Uncertainty Model $\Delta(z)$ with 1 % (520 [kg]) Mass Increase

Instead of calculating the Singular Value Decomposition along all the frequencies of interest in Figure 4.2, the case where $\Delta(z)$ has the maximum Singular Value will be considered. The maximum magnitude for $\sigma_{\max}$ of $\Delta(e^{j7.0})$ can be obtained in the Singular Value Decomposition. We define the decomposition as

$$\Delta(e^{j7.0})\Big|_{mass=1\%} = U_{m1}\,\Sigma_{m1}\,V_{m1}^{*}.$$

If we substitute $\omega = 7.0$ into $\mathbf{G}(e^{j\omega})$ in Appendix C and $\mathbf{G}_a(e^{j\omega})_{mass=1\%}$, $\Delta(e^{j7.0})\Big|_{mass=1\%}$ can be obtained from Equation (4.3);

$$\Delta(e^{j7.0})\Big|_{mass=1\%} = \begin{bmatrix} -0.0708-0.1193j & 0.0130+0.0026j & 0.1580+1.0062j \\ 0.0200-0.0225j & -0.0865+0.0833j & 0.1016-0.0300j \\ -0.0834-0.0481j & 0.0031-0.0007j & 0.1408+0.2781j \end{bmatrix}$$

By the Singular Value Decomposition for $\Delta(e^{j7.0})\Big|_{mass=1\%}$, U_{m1} will be

$$\begin{aligned} U_{m1} &= \begin{bmatrix} U_{m1,\max} & U_{m1,mid} & U_{m1,\min} \end{bmatrix} \\ &= \begin{bmatrix} -0.5106-0.8012j & 0.0180+0.0389j & 0.2367+0.1987j \\ -0.0709+0.0601j & -0.6862+0.7044j & -0.1078+0.1127j \\ -0.2311-0.1879j & 0.1618+0.0703j & -0.8756-0.3369j \end{bmatrix}, \end{aligned}$$

Σ_{m1} will be

$$\Sigma_{m1} = \begin{bmatrix} \sigma_{m1,\max} & 0 & 0 \\ 0 & \sigma_{m1,mid} & 0 \\ 0 & 0 & \sigma_{m1,\min} \end{bmatrix} = \begin{bmatrix} 1.0819 & 0 & 0 \\ 0 & 0.1301 & 0 \\ 0 & 0 & 0.0488 \end{bmatrix},$$

and V_{m1} will be

$$\begin{aligned} V_{m1} &= \begin{bmatrix} V_{m1,\max} & V_{m1,mid} & V_{m1,\min} \end{bmatrix} \\ &= \begin{bmatrix} 0.1454 & -0.4027 & 0.9037 \\ 0.0017-0.0084j & 0.9132-0.0231j & 0.4067-0.0089j \\ -0.9064+0.3965j & -0.0495+0.0301j & 0.1238-0.0504j \end{bmatrix}. \end{aligned}$$

The above Singular Value Decomposition means that if

$$\mathbf{u} = V_{m1,\max} = \begin{bmatrix} 0.1454 \\ 0.0017-0.0084j \\ -0.9064+0.3965j \end{bmatrix},$$

the output will be

$$\mathbf{y} = \sigma_{m1,\max} U_{m1,\max} = 1.0819 \begin{bmatrix} -0.5106-0.8012j \\ -0.0709+0.0601j \\ -0.2311-0.1879j \end{bmatrix} = \begin{bmatrix} -0.5524-0.8668j \\ -0.0767+0.0650j \\ -0.2500-0.2033j \end{bmatrix}. \qquad (4.4)$$

On the other hand, the Singular Value Decomposition for the nominal model $\mathbf{G}(z)$ at the same frequency can be define as

$$\mathbf{G}(e^{j7.0}) = U_G \Sigma_G V_G^* .$$

If we substitute $\omega = 7.0$ into $\mathbf{G}(e^{j\omega})$ in Appendix C, $\mathbf{G}(e^{j7.0})$ will be

$$\mathbf{G}(e^{j7.0}) = \begin{bmatrix} -10.9990 - 12.9412\text{j} & -0.2203 + 0.4728\text{j} & 2.9353 + 15.8930\text{j} \\ -1.4298 + 0.4482\text{j} & 9.9854 - 9.4613\text{j} & 2.4379 - 1.1657\text{j} \\ -6.7775 - 3.3851\text{j} & 0.4933 - 0.1549\text{j} & 1.9691 + 3.8661\text{j} \end{bmatrix}.$$

By the Singular Value Decomposition for $\mathbf{G}(e^{j7.0})$, U_{m1} will be

$$\begin{aligned} U_G &= \begin{bmatrix} U_{G,\max} & U_{G,mid} & U_{G,\min} \end{bmatrix} \\ &= \begin{bmatrix} -0.5989 - 0.7071\text{j} & 0.1483 + 0.0564\text{j} & 0.2801 + 0.1942\text{j} \\ -0.1181 + 0.1169\text{j} & -0.3684 + 0.9136\text{j} & 0.0409 + 0.0187\text{j} \\ -0.2964 - 0.1608\text{j} & 0.0476 + 0.0470\text{j} & -0.9078 - 0.2404\text{j} \end{bmatrix}, \end{aligned}$$

Σ_G will be

$$\Sigma_G = \begin{bmatrix} \sigma_{G,\max} & & \\ & \sigma_{G,mid} & \\ & & \sigma_{G,\min} \end{bmatrix} = \begin{bmatrix} 25.1881 & 0 & 0 \\ 0 & 13.6667 & 0 \\ 0 & 0 & 1.9917 \end{bmatrix},$$

and V_G will be

$$\begin{aligned} V_G &= \begin{bmatrix} V_{G,\max} & V_{G,mid} & V_{G,\min} \end{bmatrix} \\ &= \begin{bmatrix} 0.7350 & -0.1395 & 0.6636 \\ -0.1036 + 0.0145\text{j} & -0.9009 + 0.4086\text{j} & -0.0746 + 0.0699\text{j} \\ -0.5807 + 0.3342\text{j} & -0.0261 - 0.0355\text{j} & 0.6376 - 0.3776\text{j} \end{bmatrix}. \end{aligned}$$

From the above computation, we can see that the maximum Singular Value for the nominal model $\sigma_{G\max}$ (25.1881) is much greater than $\sigma_{m1,\max}$ (1.0819). In Equation (4.4) each element shows the effect to the corresponding irregularities. To evaluate the

contribution of $\Delta(z)$, these effects should be compared with the standard of rail irregularities (Table 4.1). The standards for rail irregularities means the acceptable upper or lower bounds for rail irregularities. If an actual irregularity is the standard range, the rail must be aligned. Since norms of elements in Equation (4.4) are much smaller than the standards, the contribution of the 1% mass variation can be considered small compared to the output of the nominal model.

Table 4.1 Standards of Rail Irregularities

	Standards for Maintenance Work
Lateral Irregularity	± 4 [mm]
Vertical Irregularity	± 7 [mm]
Level Irregularity	± 5 [mm]

The acceptable upper bound of mass variation that satisfies the standards of rail irregularities should be found. Figure 4.5 shows the Singular Value Plots for the model with 7 % mass increase. The maximum Singular Value for $\Delta(z)$ in the range of interest is 7.15 at the frequency $\omega = 7.2$ [rad]. We define the decomposition as

$$\Delta(e^{j7.2})\Big|_{mass=7\%} = U_{m7}\,\Sigma_{m7}\,V_{m7}^{*}.$$

If we substitute $\omega = 7.2$ into $\mathbf{G}(e^{j\omega})$ in Appendix C and $\mathbf{G}_a(e^{j\omega})_{mass=7\%}$, $\Delta(e^{j7.2})\Big|_{mass=7\%}$ can be obtained from Equation (4.3) as

$$\Delta(e^{j7.2})\Big|_{mass=7\%} = \begin{bmatrix} -1.9071+5.7153j & 0.4696+0.0459j & 0.8488+1.3735j \\ 0.5413-0.5248j & -6.1680-1.5133j & -0.5628+0.2823j \\ 0.0742+2.5265j & -0.1721-0.2938j & 0.4964+0.2331j \end{bmatrix}$$

By the Singular Value Decomposition for $\Delta(e^{j7.2})\Big|_{mass=7\%}$, U_{m7} will be

$$U_{m7} = \begin{bmatrix} U_{m7,\max} & U_{m7,mid} & U_{m7,\min} \end{bmatrix}$$
$$= \begin{bmatrix} -0.2560+0.7002j & 0.1417-0.5255j & 0.3686-0.1099j \\ 0.3687-0.4711j & 0.4676-0.6478j & 0.0317-0.0537j \\ 0.0348+0.2917j & 0.0269-0.2546j & -0.7396+0.5487j \end{bmatrix},$$

Σ_{m7} will be

$$\Sigma_{m7} = \begin{bmatrix} \sigma_{m7,\max} & 0 & 0 \\ 0 & \sigma_{m7,mid} & 0 \\ 0 & 0 & \sigma_{m7,\min} \end{bmatrix} = \begin{bmatrix} 7.1561 & 0 & 0 \\ 0 & 5.9995 & 0 \\ 0 & 0 & 0.1802 \end{bmatrix},$$

and V_{m7} will be

$$V_{m7} = \begin{bmatrix} V_{m7,\max} & V_{m7,mid} & V_{m7,\min} \end{bmatrix}$$
$$= \begin{bmatrix} 0.7932 & -0.5537 & 0.2534 \\ -0.2433+0.5260j & -0.2985+0.7503j & 0.1093-0.0072j \\ 0.0684+0.1738j & -0.1823-0.0901j & -0.6122-0.7409j \end{bmatrix}.$$

If input $\mathbf{u}$ is in the direction of $V_{m7,\max}$, that is,

$$\mathbf{u} = V_{m7,\max} = \begin{bmatrix} 0.7932 \\ -0.2433+0.5260j \\ 0.0684+0.1738j \end{bmatrix},$$

the output will be

$$\mathbf{y} = \sigma_{m7,\max} U_{m7,\max} = 7.1561 \begin{bmatrix} -0.2560+0.7002j \\ 0.3687-0.4711j \\ 0.0348+0.2917j \end{bmatrix} = \begin{bmatrix} -1.8319+5.0109j \\ 2.6385-3.3711j \\ 0.2487+2.0873j \end{bmatrix}.$$

The norm of each element of $\mathbf{y}$ will be

$$\begin{bmatrix} \|-1.8319+5.0109j\| \\ \|2.6385-3.3711j\| \\ \|0.2487+2.0873j\| \end{bmatrix} = \begin{bmatrix} 5.33 \\ 4.28 \\ 2.10 \end{bmatrix}. \qquad (4.5)$$

Equation (4.5) shows that the output for the Lateral Irregularity is greater than the standard (+4) for the Lateral Irregularity in Table 4.1. This means that the deviation produced by 7% increase of the mass is greater than the standard in the worst case. Therefore, we cannot use the nominal model in the case where mass variation goes over 7 %.

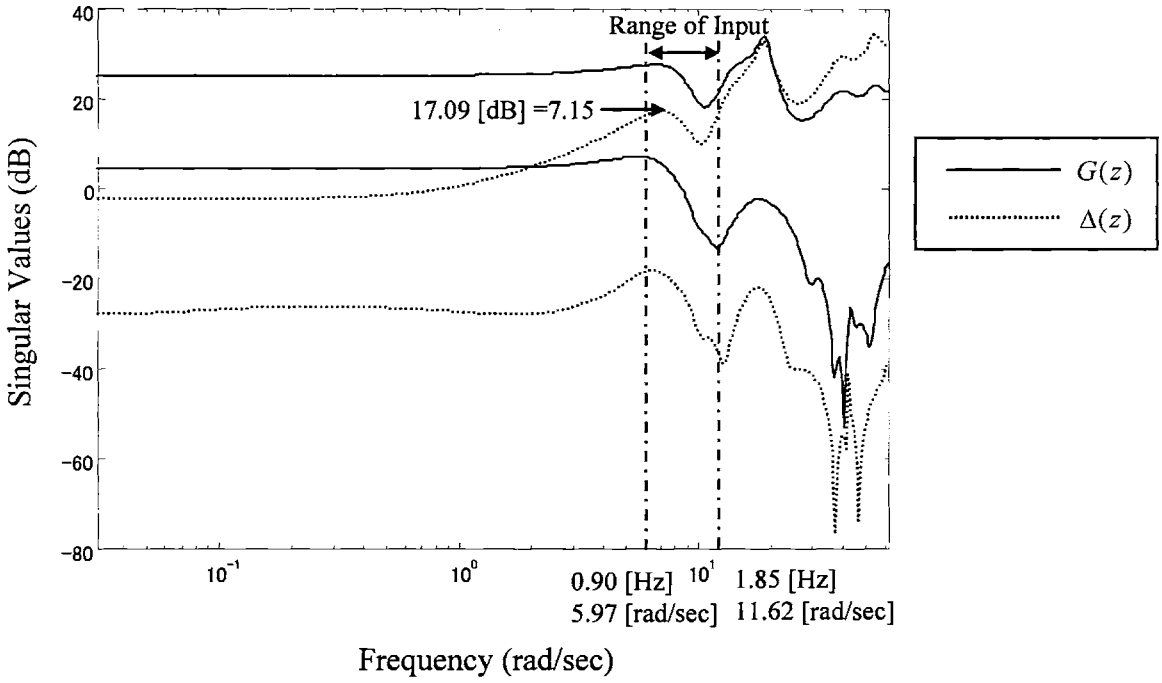

Figure 4.5 Singular Value Plots for a Nominal Model (Mass = 52000 [kg]) $G(z)$ and an Uncertainty Model $\Delta(z)$ with 7 % (3640 [kg]) Mass Increase

Table 4.2 summarizes the results of the assessment for mass variations. The more mass variation the model has, the more effect each irregularity has. Therefore, the acceptable upper bound for the nominal model is 5 % for mass variations. Typically, a Shinkansen vehicle has 100 passengers. 5 % mass increase corresponds to 32.5 passengers.

Table 4.2 Deviations by the Mass Variation

	1% 520 [kg]	5% 2600 [kg]	7% 3640 [kg]	Standard
Lateral Irregularity	1.03 [mm]	3.07 [mm]	5.33 [mm]	4 [mm]
Vertical Irregularity	0.14[mm]	2.02 [mm]	3.88 [mm]	7 [mm]
Level Irregularity	0.27 [mm]	1.85 [mm]	2.10 [mm]	5 [mm]

4.2.2 Speed Variation

Speed Variation is another main factor of model uncertainties. The speed of a vehicle ranges from 0 [km/h] to 270 [km/h] in the case of a bullet train, such as the Shinkansen.

We can assess the effect of Speed Variation in the same manner as in Subsection 4.2.1. Table 4.3 shows the results of the assessment. For 10% and 25 % speed variations, the deviation in each irregularity is smaller than the standard of rail irregularities. However, for 30 % speed variation, the deviation in the Lateral Irregularity is outside the standard. In addition, the more speed variation the model has, the more effect each irregularity has. Therefore, the acceptable upper bound for the nominal model is 25 %.

Table 4.3 Deviations by the Speed Variation

	10% (79.2[km/h])	25% (90 [km/h])	30% (93.6 [km/h])	Standard
Lateral Irregularity	1.87 [mm]	2.12 [mm]	5.79 [mm]	4 [mm]
Vertical Irregularity	1.20 [mm]	2.03 [mm]	1.62 [mm]	7 [mm]
Level Irregularity	0.89 [mm]	1.76 [mm]	2.76 [mm]	5 [mm]

4.3 A Compensation Method for System Uncertainties

From the results of Section 4.2, the effects of mass variation and speed variation are considered significant for the nominal model. We cannot use a nominal model for all situations. Therefore, compensation methods for them are needed.

Assessment for mass variation showed that the upper and lower limits of mass variation that can be covered by the nominal model were 5 % in Section 4.2. While the mass of a passenger car that has no passenger is 52,000 [kg], the mass of a passenger car that is full of passengers is 68,000 [kg]. The middle point is 60,000 [kg]. Since a nominal model covers ± 5% range from the nominal mass, we need at least three models in order to cover all the range of mass variation, as shown in Table 4.4. The first model will be constructed so that the nominal mass is 54,600 [kg]. The second model's nominal mass is 60,000 [kg], followed by the third model whose nominal mass is 65,000 [kg].

Table 4.4 Assignments of Models for the Mass Variation

Mass [kg]	52,000	54,600	57,300	60,000	62,600	65,000	68,000
Assignment of Models		No.1		No.2		No.3	

Table 4.5 shows an assignment of models for speed variation. In the same manner as the case of mass variation, 7 models are needed to cover whole the range of speed..

Table 4.5 Assignments of Models for the Speed Variation

Speed[km/h]	0	18	36	54	72	90	108
Assignment of Models	No.1 ◄——►			No.2 ◄——►		No.3 ◄——►	
	126	144	162	180	198	216	234
	No. 4 ◄——►			No.5 ◄——►		No.6 ◄——►	
	252	270	288				
	No.7 ◄——►						

The system can have mass variation and speed variation simultaneously. Therefore, 21 models (3×7) must be prepared in advance in order to cover all variations.

In practice, we must know the weight of a passenger car to make sure that the actual mass is within the uncertainty requirement. If the mass is outside the acceptable range, we have to select another model as a nominal model. For Sinkansen trains and express trains, the system that automatically checks the tickets of passengers instead of a train conductor is being researched. With this system, the exact number of passengers can be determined. Therefore, we can estimate the total weight of a vehicle. On the other hand, the speed of a vehicle is easily available from the speed meter.

4.4 Summary

This chapter presents assessment for practical implementation. It evaluates the effects of two major model uncertainties, which are mass variation and speed variation, by using the Singular Value Decomposition. Since both effects are significant for the nominal model, this chapter proposes a compensation method that prepares multiple models in order to cover all the range of mass variation and speed variation.

5 Conclusions & Recommendations

A method for estimating the rail irregularity by using accelerations of a rail vehicle's car body was presented. A MIMO system model in which inputs are accelerations and outputs are rail irregularities was constructed by using the System Identification technique and simulation data.

Comparisons between the estimate and the actual irregularity in the model validation, and quantitative analysis of the estimation error reveal the followings:

(1) The estimate of the Left Vertical Irregularity agrees well with actual Left Vertical Irregularity in both phase and magnitude. The error between the estimate and the actual irregularity is acceptable.

(2) The estimation error in the Left Lateral Irregularity is larger than in the Left Vertical Irregularity, since there is a small gap between the estimate and the actual irregularity in phase. From a practical point of view, the

(3) gap in phase is acceptable.

(4) The estimate of the Level Irregularity does not agree well with the actual Level Irregularity. The locations and the number of accelerometers need to be improved.

(5) The accuracy of the estimation is expressed by the resolution. The resolution for the Vertical Irregularity is the highest. The resolution for the Lateral Irregularity is second, followed by that for the Level Irregularity.

Uncertainties produced by speed variations and mass variations of a vehicle were assessed. Since the effects of these two variations are significant, we cannot use a

nominal model for whole the range of those variations. To compensate for these effects, this thesis proposes using multiple models to cover whole the range of the vehicle's speed and mass.

The reason that the estimation for the Lateral Irregularity was not as good as that for the Vertical Irregularity is that a vehicle's properties in the lateral direction contain non-linear factors. Therefore, non-linear models instead of the ARX model can be recommended for future work. In addition, the locations of accelerometers used to estimate the Level Irregularity more accurately should be studied.

In order to implement the method proposed by this thesis, we need field experiments using actual vehicles and rail tracks. In addition to the uncertainties that were assessed by this thesis, disturbances such as wind, the effect of passengers' movement in the vehicle, and sensor noises have to be assessed.

If the proposed method of this thesis is implemented in the future, a train will be provided information about rail irregularities, which will enable us to control a vehicle's suspensions more efficiently. An interesting area of research will be the study of how to control active suspensions by using information on rail irregularities in order to realize a smart rail vehicle.

Bibliography

1. Takeshita, K., "Inspection Method of Mid-Chord Offset Irregularity by One-Order Difference Method", J-Rail, pp331-334, 1996.
2. Nagai, K., "Implementation of Rail Inspection Vehicles Measuring Accelerations" (in Japanese), Shin Senro, pp18-20, 1997.
3. Sunaga, Y., "A Practical Use of Axlebox Acceleration to Control the Short-wave Track Irregularities on Shinkansen", RTRI Report, Vol.9, No.2, pp35-40, 1995.
4. Takeshita, K., "A Method for Track Irregularity Inspection by Asymmetrical Chord Offset Method", RTRI Report, Vol.4, No.10, pp18-24, 1990.
5. Naganuma, Y., "Track Maintenance Method Considering Dynamics of Shinkansen Rolling Stock", RTRI Report, Vol.9, No.12, pp37-42, 1995.
6. Hershey, J. et al., "Apparatus and Method for detecting defective conditions in railway vehicle wheels and rail tracks", U.S. Patent #5,433,111, 1995.
7. Turbe, J., "Process and device for the automatic recognition and detection of discontinuities and irregularities in the rails of railroad tracks", U.S. Patent #4,662,224, 1987.
8. Shirota, et all., "Method and Apparatus for Optical Method of Measuring Rail Displacement", U.S. Patent #4,181,430, 1976.
9. Takeshita, K., "Track Irregularity Inspection Method by Revenue-earning Train", RTRI Report, Vol.9, No.2, pp29-34, 1995.

10. Bryan, M., "Method and apparatus for monitoring railway defects ", U.S. Patent #5,867,404, 1999.
11. Suda, Y. et al, "New Rail Track –Structure and Maintenance of Track" (in Japanese), Nihon Tetsudo Shisestu Kyoukai, 1997.
12. Yoshimura, A., "Theories on Estimation of Original Waves of Rail Track Irregularities", RTRI Report, No.1336, 1987.
13. Iwnicki, S., "The Manchester Benchmarks for Rail Vehicle Simulation", Supplement to Vehicle System Dynamics Volume 31, Swets & Zeitlinger, 1999.
14. Nagai. M., "Dynamics and Control of Vehicles" (in Japanese), Yokendo, 1999. Goodall, R., "Active Railway Suspensions: Implementation Status and Technological Trends", Transaction of Vehicle System Dynamics, 28, pp.87-117, 1997.
15. Toffner-Clausen, S., "System Identification and Robust Control", Springer, 1996.
16. Ljung, L., "System Identification –Theory for the User", Prentice Hall, 1999.
17. Zhou, K., "Essentials of Robust Control", Prentice Hall, 1999.
18. Brown, R., "Introduction to Random Signals and Applied Kalman Filtering", Wiley, 1997
19. Bobbett, J., "Stability Analysis of Uncertain Systems with Time Delay", Master Thesis in ME of MIT, 1990.

20. Ramnath, R. et al., "Nonlinear System Analysis and Synthesis –Volume 2 Techniques and Applications", The Winter Annual Meeting of the ASME, The Charles Stark Draper Laboratory, Inc., 1980.
21. Ogata, K., "Modern Control Engineering", Prentice Hall, 1997.
22. Oppenheim, A. et al., "Signals and Systems", Prentice Hall, 1996.
23. Inman, D., "Engineering Vibration", Prentice Hall, 2000.
24. Friedland, B., "Control System Design", McGraw-Hill,1986.

Appendix A. Specifications for Properties of a Vehicle and Rails

Table A.2 Properties of Stiffness and Damping between Rails and Ground Points

		Variable	Values	Unit
Lateral Direction	Stiffness	k_{gl}	4200	kgf / mm
	Damping	c_{gl}	240	$kgf \cdot s / cm$
Vertical Direction	Stiffness	k_{gv}	18000	kgf / mm
	Damping	c_{gv}	200	$kgf \cdot s / cm$

Table A.2 Properties of Mass (E2 and TR7004A)

	Name of Component	Direction	Variable	Value	Unit	
Car body	Mass		M_c	52000	kg	
	Center of Mass		h_c	1800	mm	0: Top Surface of Rails
Bogie	Mass		M_b	2459	kg	
	Mass Moment of Inertia	Rolling	J_{br}	1900	kgm^2	$i = 0.88$ i : Radius of Gyration [m]
		Pitching	J_{bp}	1200	kgm^2	$i = 0.70$
		Yawing	J_{by}	2900	kgm^2	$i = 1.09$
	Center of Mass		h_b	509	mm	0: Top Surface of Rails
Wheelset	Mass		M_w	3987	kg	
	Mass Moment of Inertia	Rolling	J_{wr}	980	kgm^2	$i = 0.70$
		Pitching	J_{wp}	130	kgm^2	$i = 0.26$
		Yawing	J_{wy}	980	kgm^2	$i = 0.70$
	Center of Mass		h_w	430	mm	0: Top Surface of Rails

Table A.3 Properties of Suspensions of a Bogie (TR7004A)

	Name of Component	Direction	Variable	Value	Unit	
Primary Suspension	Stiffness of Support of Axlebox	Vertical	k_{pv}	85.1	*kgf / mm*	
		Lateral	k_{pl}	500	*kgf / mm*	
		Longitudinal	k_{px}	900	*kgf / mm*	
	Vertical Oil Damper	Vertical	c_{pv1}	100	*kgf*	$V = 5cm/s$
			c_{pv2}	200	*kgf*	$V = 10cm/s$
			c_{pv3}	500	*kgf*	$V = 30cm/s$
Sencondary Suspension	Stiffness of Airsprings	Vertical	k_{av1}	17.6	*kgf / mm*	No Passenger
			k_{av2}	19.2	*kgf / mm*	100% Passenger
			k_{av3}	20.7	*kgf / mm*	200% passenger
		Lateral	k_{al}	17.1	*kgf / mm*	
	Lateral Oil Damper	Lateral	c_{l1}	200	*kgf*	$V = 5cm/s$
			c_{l2}	375	*kgf*	$V = 15cm/s$
	Yaw Damper	Yawing	c_{y1}	450	*kgf*	$V = 0.6cm/s$
			c_{y2}	1200	*kgf*	$V = 6.0cm/s$
	Traction Rod	Longitudinal	k_{tx}	445	*kgf / mm*	
		Lateral	k_{tl}	10	*kgf / mm*	
	Lateral Bump Stop	Lateral	k_{bl}	150	*kgf / mm*	

Appendix B. Additional Results of Model Validation

Subsection 3.3.1 details the results of the model validation. Because Figures 3.18, 3.21, and 3.24 show the limited areas of the total validation period, Figures B.1, B.2, and B.3 are added to cover all the area.

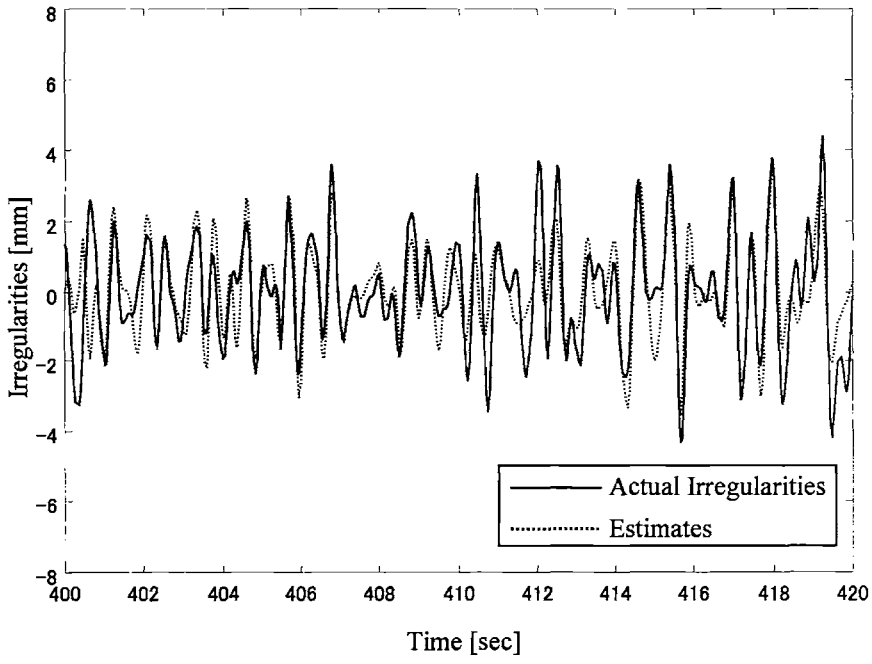

Figure B.1.1 Actual Irregularities vs. Estimates for Lateral Irregularities (from 400 [sec] to 420 [sec])

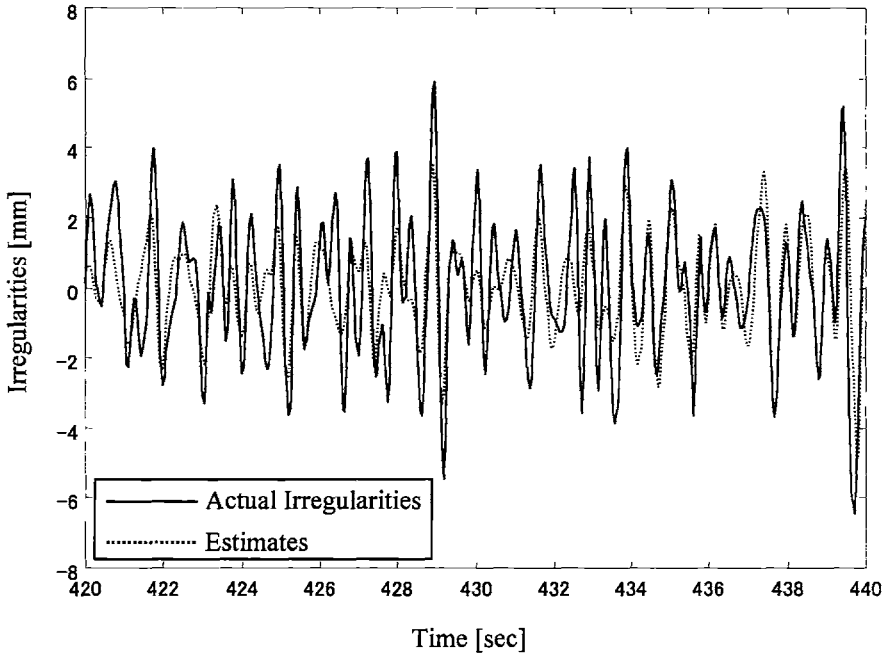

Figure B.1.2 Actual Irregularities vs. Estimates for Lateral Irregularities (from 420 [sec] to 440 [sec])

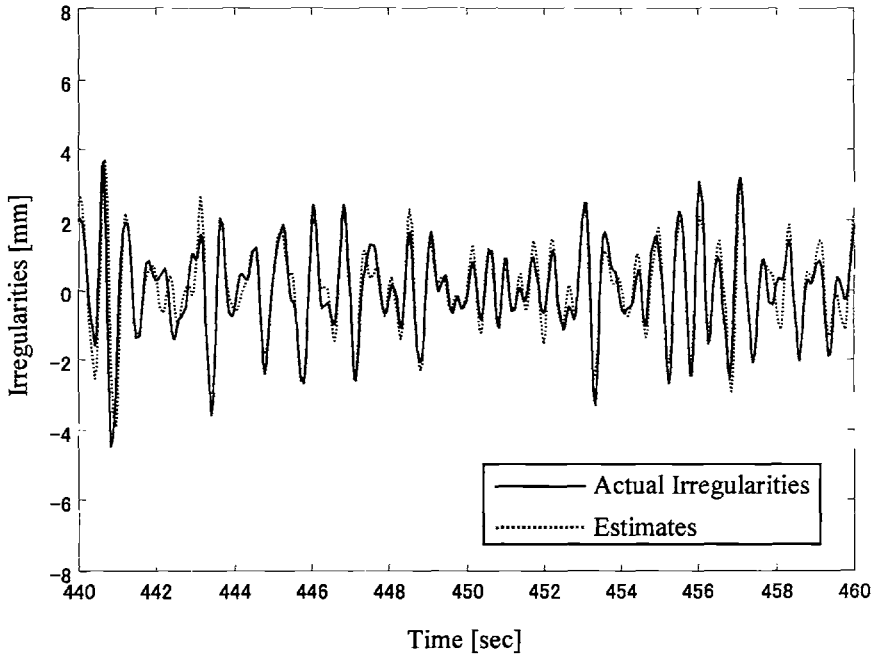

Figure B.1.3 Actual Irregularities vs. Estimates for Lateral Irregularities (from 440 [sec] to 460 [sec])

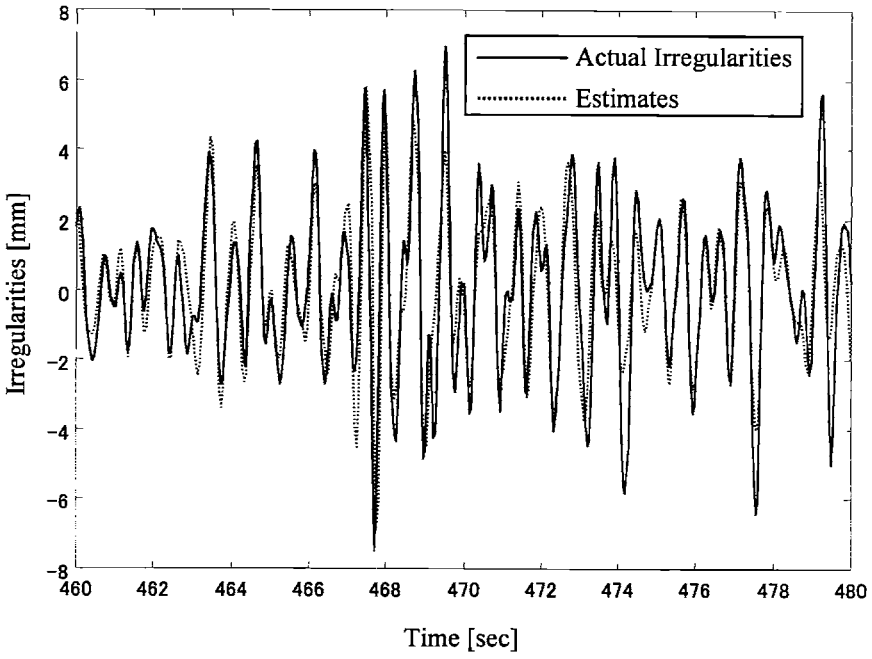

Figure B.1.4 Actual Irregularities vs. Estimates for Lateral Irregularities (from 460 [sec] to 480 [sec])

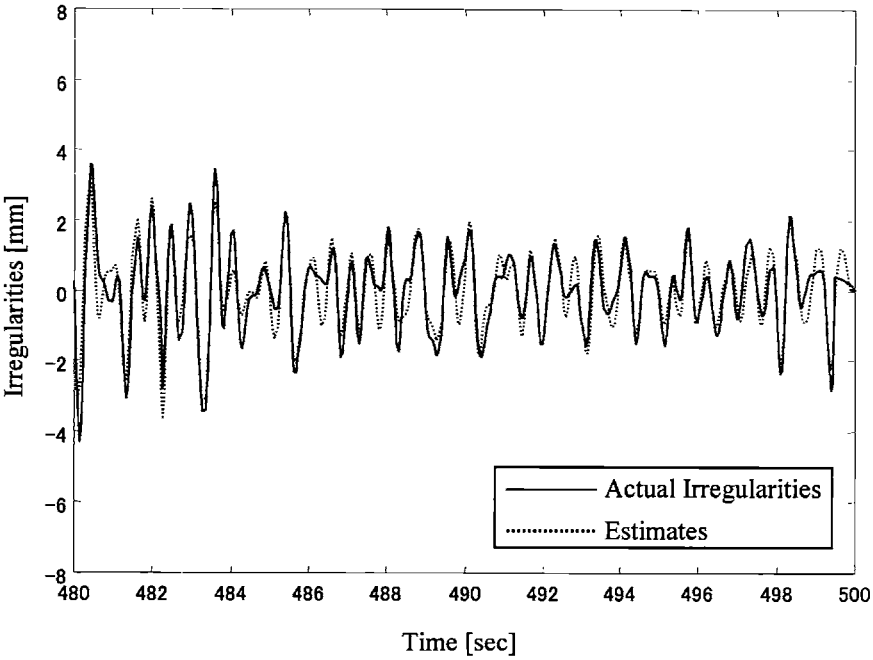

Figure B.1.5 Actual Irregularities vs. Estimates for Lateral Irregularities (from 480 [sec] to 500 [sec])

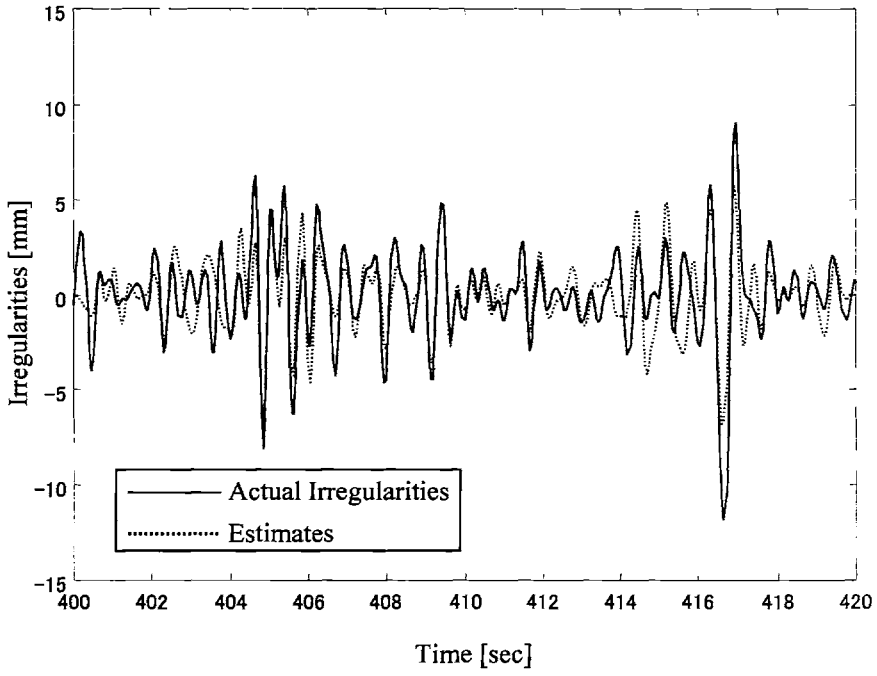

Figure B.2.1 Actual Irregularities vs. Estimates for Vertical Irregularities

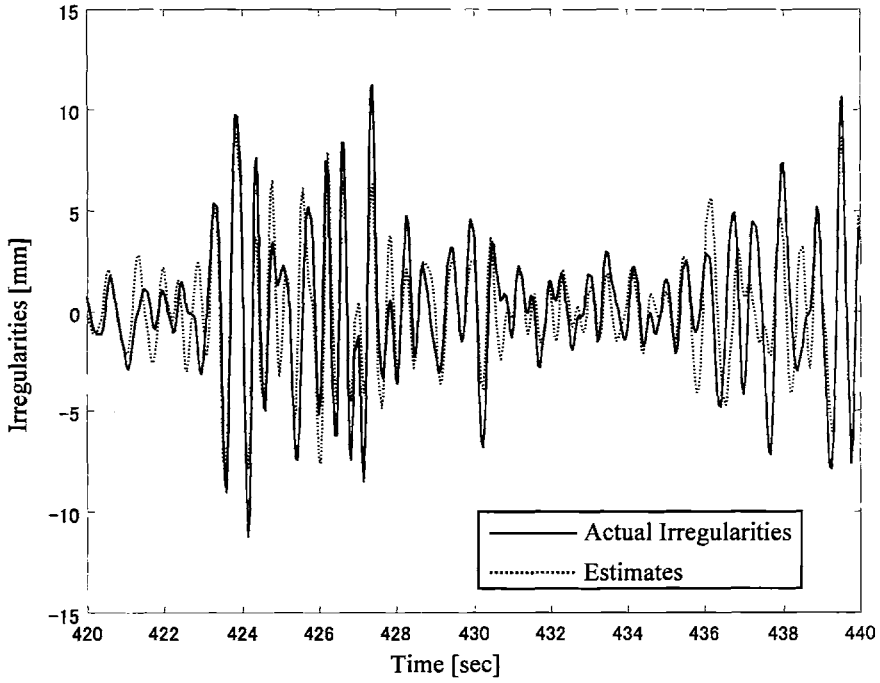

(from 400 [sec] to 420 [sec])

Figure B.2.2 Actual Irregularities vs. Estimates for Vertical Irregularities

(from 420 [sec] to 440 [sec])

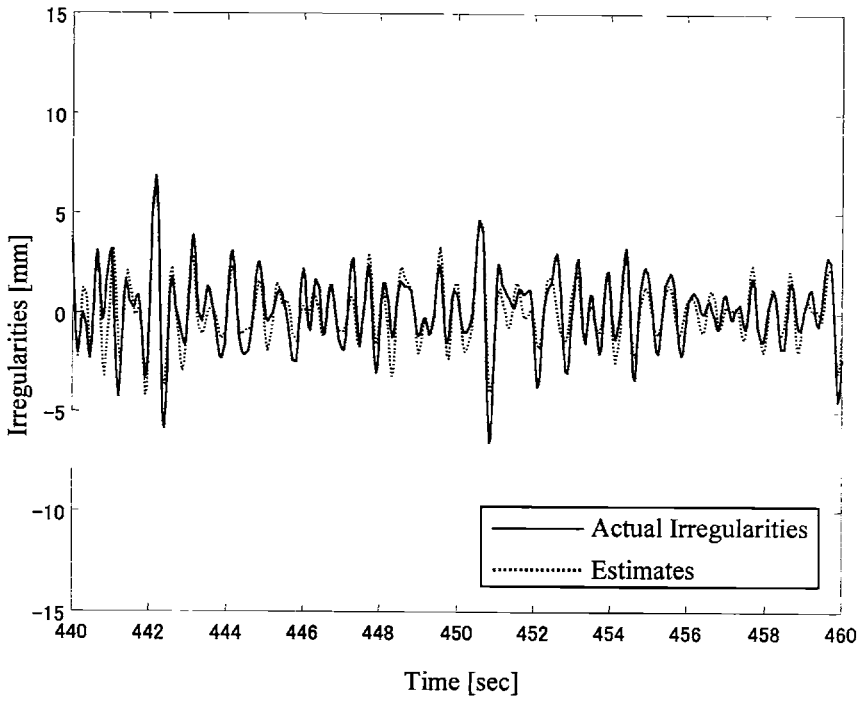

Figure B.2.3 Actual Irregularities vs. Estimates for Vertical Irregularities (from 440 [sec] to 460 [sec])

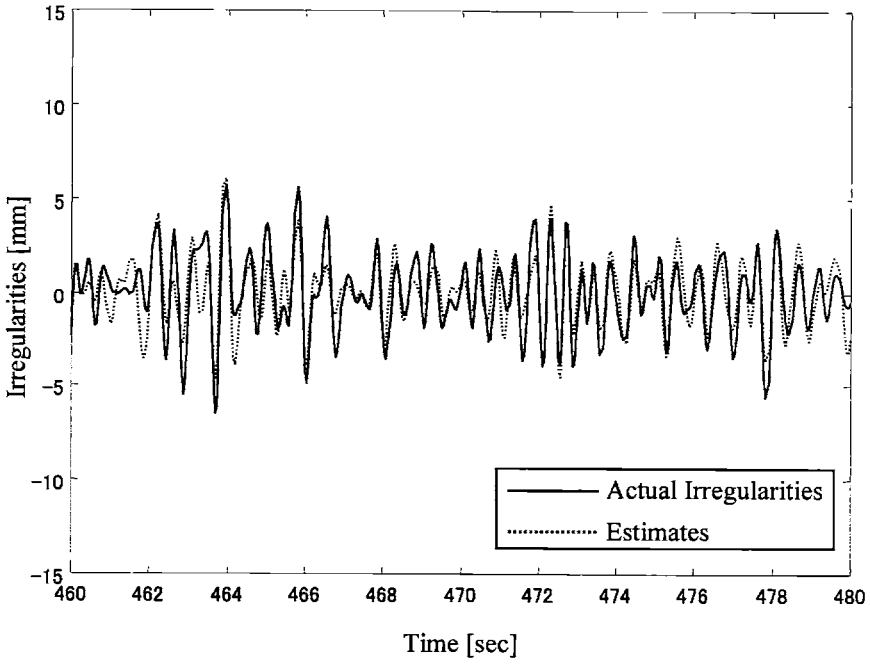

Figure B.2.4 Actual Irregularities vs. Estimates for Vertical Irregularities (from 460 [sec] to 480 [sec])

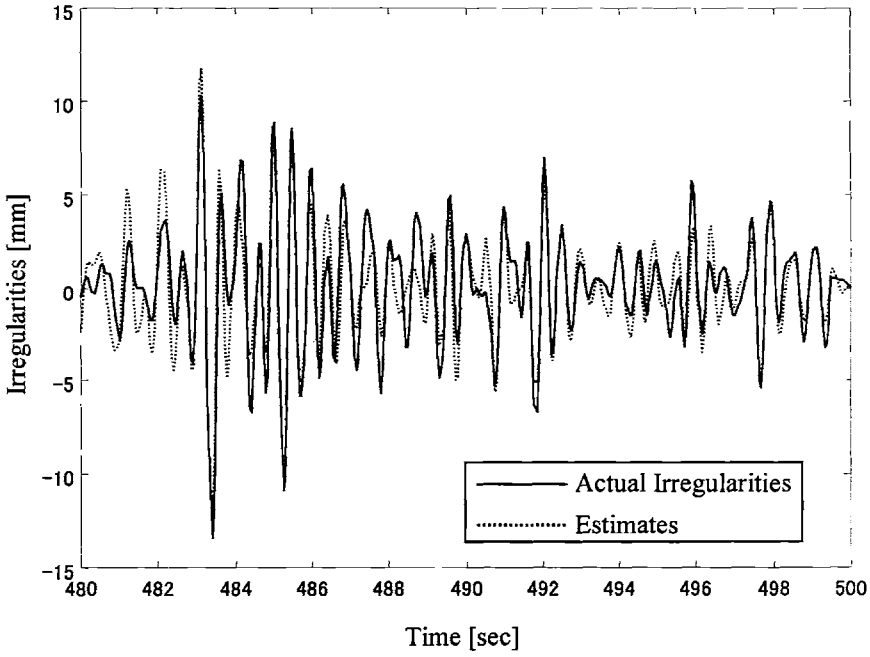

Figure B.2.5 Actual Irregularities vs. Estimates for Vertical Irregularities (from 480 [sec] to 500 [sec])

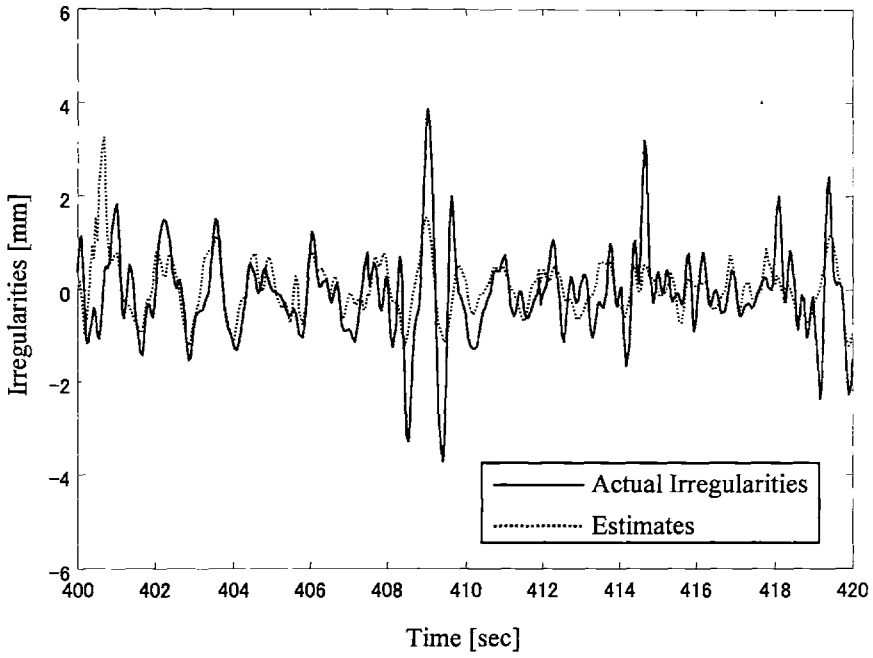

Figure B.3.1 Actual Irregularities vs. Estimates for Level Irregularities (from 400 [sec] to 420 [sec])

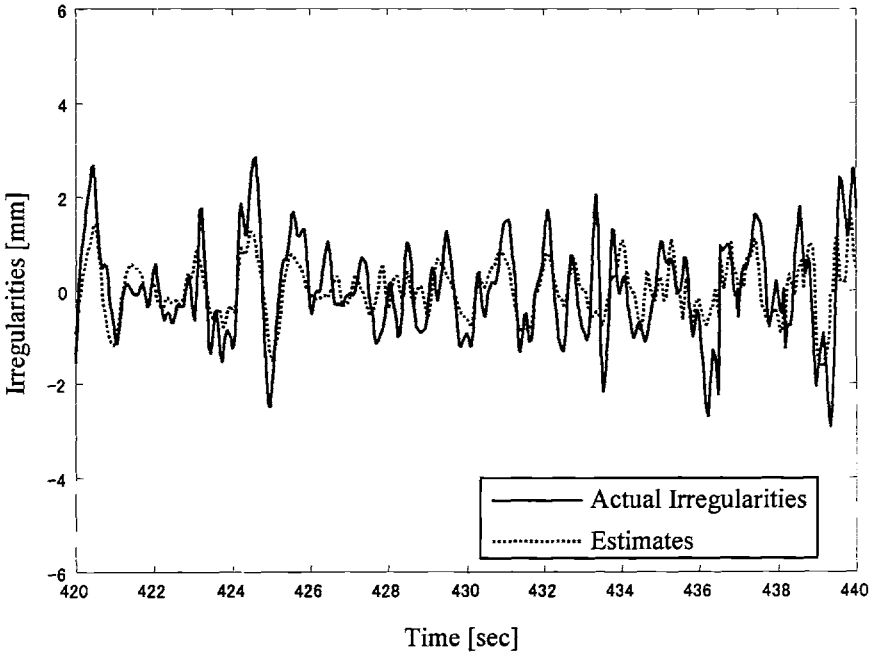

Figure B.3.2 Actual Irregularities vs. Estimates for Level Irregularities (from 420 [sec] to 440 [sec])

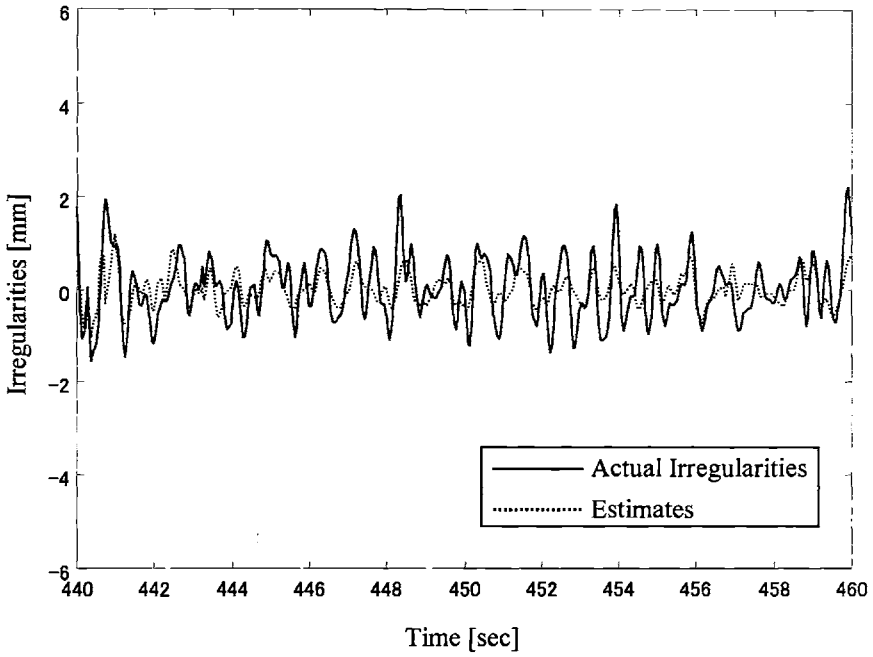

Figure B.3.3 Actual Irregularities vs. Estimates for Level Irregularities (from 440 [sec] to 460 [sec])

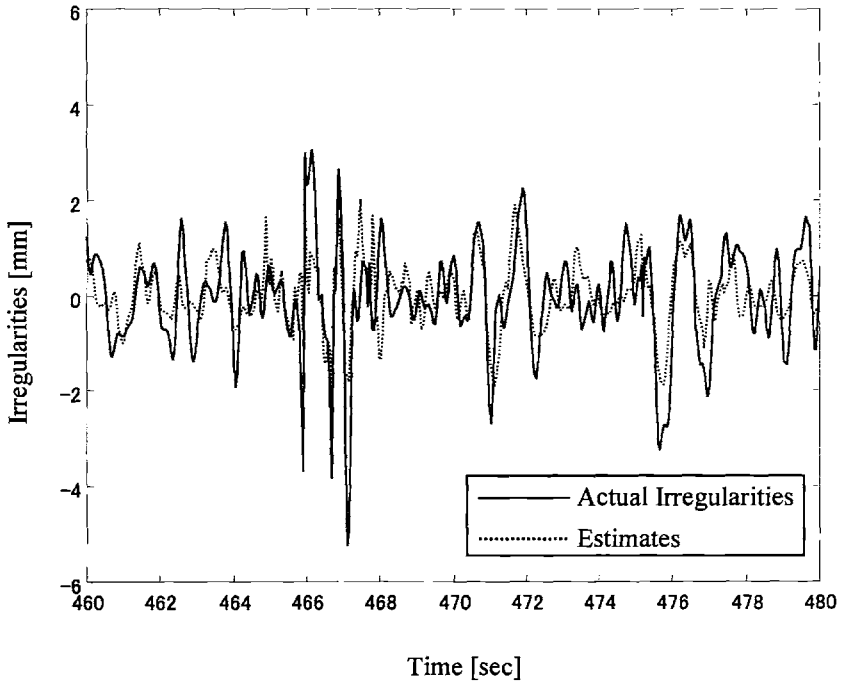

Figure B.3.4 Actual Irregularities vs. Estimates for Level Irregularities (from 460 [sec] to 480 [sec])

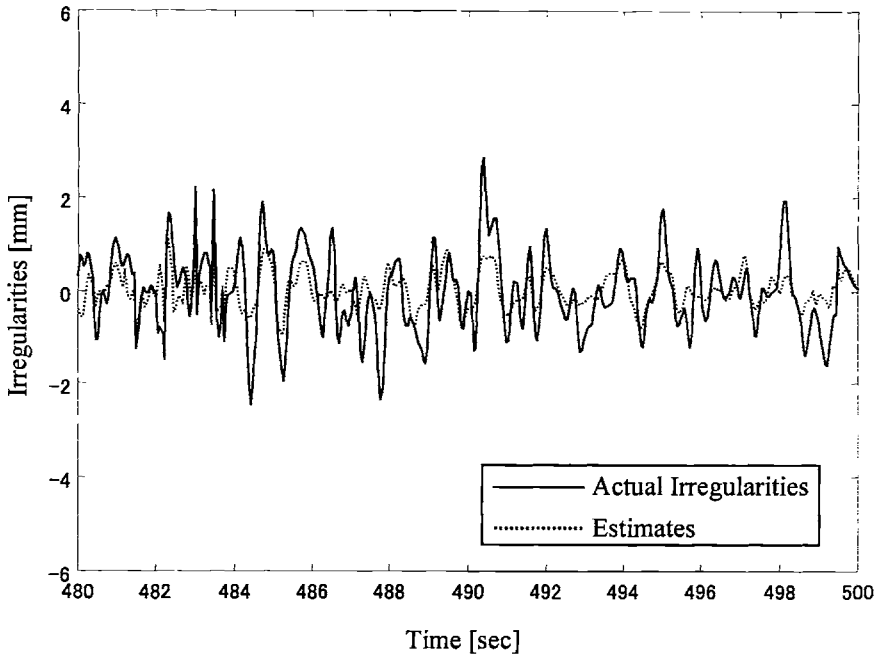

Figure B.3.5 Actual Irregularities vs. Estimates for Level Irregularities (from 480 [sec] to 500 [sec])

Appendix C. G(z) of the Inverse Model

$$G(z)=\begin{bmatrix} g_{11}(z) & g_{12}(z) & g_{13}(z) \\ g_{21}(z) & g_{22}(z) & g_{23}(z) \\ g_{31}(z) & g_{32}(z) & g_{33}(z) \end{bmatrix}$$

The denominator of all elements

= z^36 - 6.352 z^35 + 18.22 z^34 - 29.77 z^33 + 28.15 z^32 - 12.26 z^31

- 1.686 z^30 + 2.048 z^29 + 2.721 z^28 - 1.33 z^27 - 2.083 z^26

- 0.2924 z^25 + 4.434 z^24 - 3.421 z^23 - 0.1971 z^22 + 0.9767 z^21

+ 0.1576 z^20 - 0.0127 z^19 - 0.8977 z^18 + 0.8072 z^17 - 0.1002 z^16

-0.1466 z^15 + 0.003516 z^14 + 0.04896 z^13 - 0.001576 z^12 + 0.01005 z^11

-0.05032 z^10 + 0.05281 z^9 - 0.02733 z^8 + 0.007653 z^7 - 0.0009686 z^6

The numerator of g_{11}

= 0.4683 z^34 - 2.167 z^33 + 4.935 z^32 - 6.428 z^31 + 3.623 z^30 + 2.701 z^29

- 6.864 z^28 + 6.493 z^27 - 6.768 z^26 + 10.29 z^25 - 10.76 z^

+ 4.963 z^23 + 0.1223 z^22 + 0.3401 z^21 - 1.687 z^20 + 0.3189 z^19

+ 0.8227 z^18 + 0.098 z^17 - 0.7882 z^16 + 0.2012 z^15 + 0.2942 z^14

- 0.1706 z^13 + 0.08916 z^12 - 0.2084 z^11 + 0.2391 z^10 - 0.1504 z^9

+ 0.07027 z^8 - 0.02858 z^7 + 0.00925 z^6 - 0.001911 z^5 - 3.54e-016 z^4

-2.996e-016 z^3 - 1.021e-016 z^2 + 4.852e-016 z - 3.475e-016

The numerator of g_{12}

= 0.3077 z^36 - 1.502 z^35 + 2.182 z^34 + 2.212 z^33 - 12.8 z^32 + 20.61 z^31

- 16.29 z^30 + 5.753 z^29 - 3.53 z^28 + 10.7 z^27 - 13.67 z^26

+ 5.708 z^25 + 3.912 z^24 - 5.117 z^23 + 0.631 z^22 + 0.9894 z^21

+ 1.4 z^20 - 2.431 z^19 + 0.4207 z^18 + 1.105 z^17 - 0.4452 z^16

- 0.423 z^15 + 0.3012 z^14 - 0.1437 z^13 + 0.4922 z^12 - 0.7426 z^11

+ 0.5528 z^10 - 0.2311 z^9 + 0.05301 z^8 - 0.005293 z^7 - 2.967e-015 z^6

+ 2.568e-015 z^5 - 3.341e-015 z^4 + 1.969e-015 z^3 - 4.458e-017 z^2

-6.198e-016 z + 3.843e-016

The numerator of g_{13}

= -0.1096 z^35 - 0.05431 z^34 + 0.8361 z^33 - 0.9699 z^32 - 0.7234 z^31

+ 2.302 z^30 - 2.254 z^29 + 2.575 z^28 - 4.259 z^27 + 5.515 z^26

- 6.524 z^25 + 7.695 z^24 - 5.877 z^23 + 0.644 z^22 + 2.159 z^21

- 0.3061 z^20 - 1.166 z^19 - 0.1246 z^18 + 0.8272 z^17 + 0.3099 z^16

- 0.8913 z^15 + 0.2158 z^14 + 0.2519 z^13 - 0.1297 z^12 + 0.09191 z^11

- 0.2377 z^10 + 0.255 z^9 - 0.1362 z^8 + 0.03825 z^7 - 0.004464 z^6

- 9.227e-016 z^5 + 1.518e-015 z^4 - 9.718e-016 z^3 + 2.295e-016 z^2

+ 2.099e-017 z + 1.698e-017

The numerator of g_{21}

= -0.01861 z^34 + 0.07333 z^33 - 0.1217 z^32 + 0.08609 z^31 - 0.007686 z^30

+ 0.05029 z^29 - 0.2364 z^28 + 0.3378 z^27 - 0.2054 z^26 + 0.03682 z^25

- 0.07536 z^24 + 0.2096 z^23 - 0.1873 z^22 + 0.04417 z^21 + 0.02928 z^20

- 0.04402 z^19 + 0.09656 z^18 - 0.1398 z^17 + 0.1046 z^16 - 0.04146 z^15

+ 0.01263 z^14 - 0.01113 z^13 + 0.01395 z^12 - 0.01832 z^11 + 0.02132 z^10

- 0.01902 z^9 + 0.01274 z^8 - 0.006142 z^7 + 0.001735 z^6 - 0.0002961 z^5

+ 7.467e-016 z^4 - 5.506e-016 z^3 + 1.616e-016 z^2 + 5.99e-017 z - 1.156e-016

The numerator of g_{22}

= -0.2515 z^36 + 2.28 z^35 - 6.342 z^34 + 7.547 z^33 - 2.976 z^32 + 0.01058 z^31

- 3.561 z^30 + 6.15 z^29 - 5.345 z^28 + 9.642 z^27 - 16.19 z^26

+ 12.17 z^25 - 1.348 z^24 - 1.744 z^23 - 1.932 z^22 + 2.335 z^21

- 0.3326 z^20 + 1.361 z^19 - 3.211 z^18 + 2.286 z^17 - 0.3991 z^16

- 0.07715 z^15 - 0.1613 z^14 + 0.09977 z^13 + 0.0286 z^12 + 0.03808 z^11

- 0.1159 z^10 + 0.0905 z^9 - 0.03409 z^8 + 0.005656 z^7 + 6.716e-016 z^6

- 1.491e-015 z^5 + 1.361e-015 z^4 - 6.591e-016 z^3 + 2.735e-017 z^2

+ 1.982e-016 z - 1.383e-016

The numerator of g_{23}

= -0.01582 z^35 + 0.2228 z^34 - 0.6922 z^33 + 0.8782 z^32 - 0.365 z^31 - 0.07591 z^30

- 0.2002 z^29 + 0.5224 z^28 - 0.654 z^27 + 1.356 z^26 - 2.131 z^25

+ 1.626 z^24 - 0.3813 z^23 - 0.06817 z^22 - 0.1531 z^21 + 0.1428 z^20

- 0.02956 z^19 + 0.1811 z^18 - 0.3107 z^17 + 0.2001 z^16 - 0.05968 z^15

+ 0.02202 z^14 - 0.01189 z^13 - 0.005189 z^12 + 0.009154 z^11

- 0.004835 z^10 + 0.002659 z^9 - 0.001241 z^8 + 0.0002052 z^7

+ 8.153e-005 z^6 + 9.256e-017 z^5 - 6.879e-017 z^4 + 8.909e-017 z^3

- 2.044e-016 z^2 + 7.649e-017 z + 1.362e-016

The numerator of g_{31}

= 0.2423 z^34 - 0.9947 z^33 + 2.372 z^32 - 5.208 z^31 + 10.01 z^30 - 12.98 z^29

+ 9.395 z^28 - 2.911 z^27 + 0.1502 z^26 + 3.72 z^25 - 15.57 z^24

+ 24.69 z^23 - 16.88 z^22 + 1.319 z^21 + 3.311 z^20 + 1.185 z^19

- 1.197 z^18 - 3.224 z^17 + 3.346 z^16 + 0.3978 z^15 - 1.797 z^14

+ 0.4427 z^13 + 0.2936 z^12 + 0.1043 z^11 - 0.1995 z^10 - 0.1854 z^9

+ 0.3801 z^8 - 0.253 z^7 + 0.08462 z^6 - 0.01243 z^5 + 8.136e-016 z^4

- 1.937e-016 z^3 + 7.86e-018 z^2 - 2.705e-016 z + 3.288e-016

The numerator of g_{32}

= 0.5514 z^36 - 4.541 z^35 + 16.83 z^34 - 34.62 z^33 + 38.4 z^32 - 16.87 z^31

+ 14.59 z^30 - 107.4 z^29 + 280.1 z^28 - 383.3 z^27 + 302 z^26

- 119.5 z^25 + 6.952 z^24 + 1.996 z^23 - 3.318 z^22 + 37.66 z^21

- 51.57 z^20 + 20.77 z^19 + 10.42 z^18 - 11.3 z^17 + 0.7756 z^16

+ 0.768 z^15 + 1.324 z^14 + 1.323 z^13 - 5.144 z^12 + 5.17 z^11

- 2.695 z^10 + 0.7732 z^9 - 0.1044 z^8 + 0.002671 z^7 + 7.332e

-015 z^6 + 5.396e-016 z^5 - 3.954e-015 z^4 + 3.211e-015 z^3 - 1.329e-015 z^2

+ 1.224e-016 z + 1.871e-016

The numerator of g_{33}

= -0.05511 z^35 - 0.6522 z^34 + 4.363 z^33 - 10.57 z^32 + 12.44 z^31 - 7.295 z^30

+ 9.166 z^29 - 33.96 z^28 + 71.2 z^27 - 90.27 z^26 + 76.55 z^25

- 44.54 z^24 + 16.14 z^23 - 0.5829 z^22 - 5.397 z^21 + 8.049 z^20

- 9.093 z^19 + 6.448 z^18 - 1.114 z^17 - 2.11 z^16 + 1.512 z^15

- 0.0632 z^14 - 0.2483 z^13 + 0.373 z^12 - 0.9549 z^11 + 1.243 z^10

- 0.8771 z^9 + 0.3563 z^8 - 0.07974 z^7 + 0.007779 z^6 + 1.005e-015 z^5

- 1.172e-015 z^4 + 1.469e-015 z^3 - 1.535e-015 z^2 + 1.011e-015 z - 3.79e-016

Appendix D. Matlab Codes for the Singular Value Plot

```
Ts=0.05;
[num_g1,den_g]=th2tf(S0_10101,1);
[num_g2,den_g]=th2tf(S0_10101,2);
[num_g3,den_g]=th2tf(S0_10101,3);
[num_m1,den_m]=th2tf(S5_10101,1);
[num_m2,den_m]=th2tf(S5_10101,2);
[num_m3,den_m]=th2tf(S5_10101,3);

g11=tf(num_g1(1,:),den_g,Ts);
g21=tf(num_g1(2,:),den_g,Ts);
g31=tf(num_g1(3,:),den_g,Ts);
g12=tf(num_g2(1,:),den_g,Ts);
g22=tf(num_g2(2,:),den_g,Ts);
g32=tf(num_g2(3,:),den_g,Ts);
g13=tf(num_g3(1,:),den_g,Ts);
g23=tf(num_g3(2,:),den_g,Ts);
g33=tf(num_g3(3,:),den_g,Ts);

m11=tf(num_m1(1,:),den_m,Ts);
m21=tf(num_m1(2,:),den_m,Ts);
```

```
m31=tf(num_m1(3,:),den_m,Ts);
m12=tf(num_m2(1,:),den_m,Ts);
m22=tf(num_m2(2,:),den_m,Ts);
m32=tf(num_m2(3,:),den_m,Ts);
m13=tf(num_m3(1,:),den_m,Ts);
m23=tf(num_m3(2,:),den_m,Ts);
m33=tf(num_m3(3,:),den_m,Ts);

sysG=[g11 g12 g13;
    g21 g22 g23;
    g31 g32 g33];

sysM=[m11 m12 m13;
    m21 m22 m23;
    m31 m32 m33];

sysDelta=sysM-sysG;
NF=pi/Ts; %Nyquist Freq
W=logspace(-1.5,log10(NF),500);
sigma(sysG,W);
hold on
sigma(sysDelta,W);
hold off
```